Article

The Composition of Zircon and Igneous and Metamorphic Petrogenesis

HOSKIN, P. W. O., SCHALTEGGER, Urs

The Composition of Zircon and Igneous and Metamorphic Petrogenesis

Paul W. O. Hoskin

Institut für Mineralogie, Petrologie und Geochemie, Albert-Ludwigs-Universität Freiburg
D-79104 Freiburg, Germany

Urs Schaltegger

Section des Sciences de la Terre, Départment de Minéralogie, Rue des Maraîchers 13
CH-1211 Genève 4, Switzerland

INTRODUCTION

Zircon is the main mineral in the majority of igneous and metamorphic rocks with Zr as an essential structural constituent. It is a host for significant fractions of the whole-rock abundance of U, Th, Hf, and the REE (Sawka 1988, Bea 1996, O'Hara et al. 2001). These elements are important geochemically as process indicators or parent isotopes for age determination. The importance of zircon in crustal evolution studies is underscored by its predominant use in U-Th-Pb geochronology and investigations of the temporal evolution of both the crust and lithospheric mantle. In the past decade an increasing interest in the composition of zircon, trace-elements in particular, has been motivated by the effort to better constrain *in situ* microprobe-acquired isotopic ages. Electron-beam compositional imaging and isotope-ratio measurement by *in situ* beam techniques—and the micrometer-scale spatial resolution that is possible—has revealed in many cases that single zircon crystals contain a record of multiple geologic events. Such events can either be zircon-consuming, alteration, or zircon-forming and may be separated in time by millions or billions of years. In many cases, calculated zircon isotopic ages do not coincide with ages of geologic events determined from other minerals or from whole-rock analysis. To interpret the geologic validity and significance of multiple ages, and ages unsupported by independent analysis of other isotopic systems, has been the impetus for most past investigations of zircon composition. Some recent compositional investigations of zircon have not been directly related to geochronology, but to the ability of zircon to influence or record petrogenetic processes in igneous and metamorphic systems.

Sedimentary rocks may also contain a significant fraction of zircon. Although authigenic zircon has been reported (Saxena 1966, Baruah et al. 1995, Hower et al. 1999), it appears to be very rare and may in fact be related to externally-sourced hydrothermal fluids. Sedimentary zircon is predominantly derived from weathered igneous and metamorphic rocks. Detrital zircon in sedimentary rocks and sediments is highly durable and records age information of crustal units that contributed to the sediment load. In mature sediments where zircon may be one of a few, or the only, remaining heavy-mineral, information on source-rock compositions is largely lost, and may only be attainable through interpretation of zircon composition. The use of zircon trace-element composition as a provenance indicator of detrital zircon—or xenocrystic zircon—will be reviewed in this chapter.

This chapter reviews investigations on the composition of igneous and metamorphic zircon and its role in understanding the petrogenesis of such rocks. Hydrothermal zircon will also be discussed, although there is presently little known about this potentially significant petrogenesis. A growing data-base and understanding of zircon composition is directly related to advances in analytical technology and these are summarized next for where these technologies and techniques have been applied to zircon analysis.

1529-6466/03/0053-0002$05.00

Analytical techniques

Analytical techniques where a bulk sample of small crystals, separated from a large volume of rock, are still often used for zircon compositional analysis (Gromet and Silver 1983, Mahood and Hildreth 1983, Murali et al. 1983, Fujimaki 1986, Rupasinghe and Dissanayake 1987, Sawka 1988, Heaman et al. 1990, Wiedenbeck et al. 1995). Such bulk techniques include instrumental neutron activation analysis (INAA), isotope dilution thermal ionization spectrometry (ID-TIMS) and solution inductively coupled plasma mass spectrometry (ICP-MS). Minimum sample size ranges from a few crystals to hundreds-of-milligrams and analyses, therefore, represent an "average" which may include two or more internal structures or mineral and melt inclusions. Often, analyses of zircon by INAA or TIMS have greater abundances of the REE (light REE in particular), Th, U, and possibly Ca, Nb, Ta, and other elements, relative to *in situ* microprobe techniques (Fig. 1). For INAA analyses this may be due to the presence of fission-derived light REE, but for most cases it is likely related to the presence of inclusions which are commonly recorded for zircon (Gorz 1974, Chesner 1998, Thomas et al. 2002). In a study of the composition of a large cm-sized, gem-quality zircon, Jain et al. (2001) attributed increased LREE, Nb, Y, Th, and U abundances relative to *in situ* analyses of fractions of the same crystal to the presence of pyrochlore inclusions. Sano et al. (2002) report anomalously high LREE abundances in their INAA and TIMS analyses due to the presence of 1-5 μm-sized apatite inclusions—their *in situ* microprobe analyses of the same zircon crystals did not have anomalous LREE abundances. This chapter will concentrate on data obtained by *in situ*

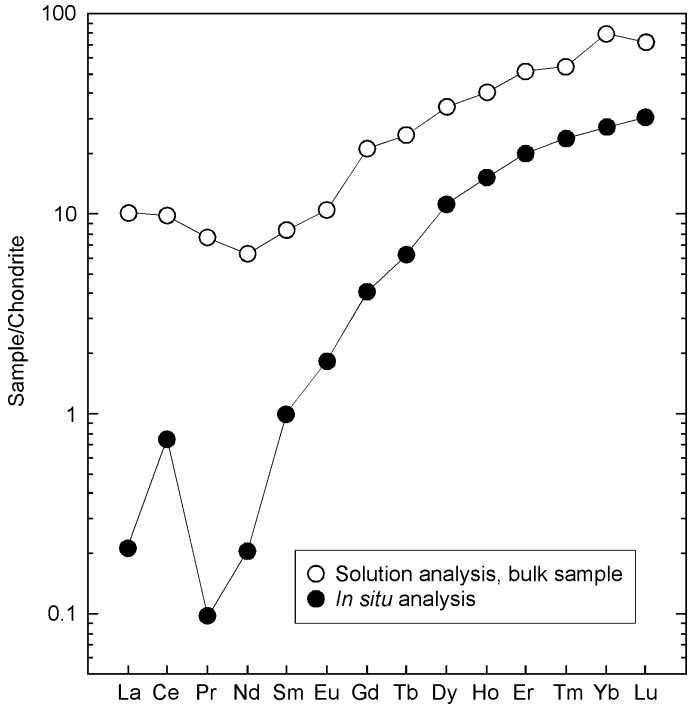

Figure 1. Chondrite-normalized plots of average zircon composition determined by *in situ* analysis (laser ablation ICP-MS) and bulk sample solution analysis (ICP-MS). Chips of the same zircon were analyzed. The difference between the two plots is due to unintentional analysis of clear, optically unobserved, mineral inclusions in the solution analysis. This style of pattern (elevated LREE, loss of positive Ce anomaly) is commonly observed for zircon analyses by bulk techniques and is not representative of the zircon composition. Data from Jain et al. (2001).

microprobe techniques where the reported data does not include accidental analysis of inclusions as part of the zircon analysis.

The analysis of zircon in thin-section or grain-mount by a microprobe allows for data acquisition from texturally distinct areas within single crystals. Textural imaging using cathodoluminesence (CL) or back-scattered electrons (BSE) is usually done prior to analysis. The electron microprobe (EMP) remains the most common instrument for compositional analysis, but ion-beam and laser-beam microprobe techniques are preferred above the EMP for trace-element analysis because of better detection limits and analytical precision. Techniques for and accurate and precise trace-element analyses of zircon by secondary ion mass spectrometry (SIMS) were first published in the late 1980s and early 1990s (Zinner and Crozaz 1986, Hinton and Meyer 1991, Hinton and Upton 1991, Ireland and Wlotzka 1992, Maas et al. 1992). This technique requires high mass-resolution or reasonably strong energy-filtering yet retention of high ion transmission. Analysis by SIMS, then, requires a large ion-probe and for nearly two decades these were only accessible in a few laboratories worldwide. Although the number of large ion-probe facilities has increased, the introduction of stable plasma-based analysis has meant that rapid, high-quality isotope and trace-element data can be acquired by a spatially resolved laser-beam microprobe. Early analyses of zircon by inductively coupled plasma mass spectrometry (ICP-MS) with sample introduction by a laser-ablation (LA) microprobe were published in the early and mid-1990s (Perkins et al. 1992, Jackson et al. 1992, Feng et al. 1993, Hirata and Nesbitt 1995, Jeffries et al. 1996). Most of the earliest studies of zircon using LA–ICP-MS focused on geochronology, attempting to develop the technology as an alternative to SIMS analysis. Hoskin (1998) was first to compare SIMS and LA–ICP-MS for zircon trace-element analysis, concluding that the techniques were competitive in terms of accuracy and precision (~5-15%), lower-limits of detection (sub-ppm for most elements), and maximum sample-surface spatial resolution (10-50 μm). Laser-ablation sampling, which excavates a pit tens-of-micrometers into the sample, may encounter inclusions which compromise data quality. SIMS data are much less prone to accidental inclusion analysis. Focused soft (Shnyukov et al. 2002) and hard (Blagojevic et al. 2000, Yusoff 2002) X-ray beams are also utilized for zircon compositional analysis and element-distribution mapping. The advantage of synchrotron radiation in particular, is the high spatial resolution (10 μm) and detection-limits (ppm to sub-ppm) that can be used non-destructively on zircon crystal interiors or surfaces.

ZIRCON AND IGNEOUS PETROGENESIS

Saturation, crystallization, occurrences and zoning of igneous zircon

Saturation and dissolution. Many workers refer to the ubiquity of zircon in crustal rocks and indeed its occurrence is widespread. However, zircon is not ubiquitous as it does not occur in every crustal rock; it is most common in igneous rocks of intermediate to Si-saturated composition and least common in less saturated rocks. The relation between zircon saturation, crystallization and melt composition was investigated by Watson (1979) and revisited by Watson and Harrison (1983). The experimental saturation relation is most commonly used for the calculation of zircon saturation temperatures for natural rocks, which are used to assess whether or not zircon was an early or late crystallizing phase. An assessment of the use of saturation temperatures is given by Hanchar and Watson (this volume). Dickinson and Hess (1982) determined from experiment that early zircon saturation (at 1100°C) in lunar granites would require the granites to have a whole-rock Zr abundance of 5000 ppm and late-stage lunar basalts to have 9000 ppm Zr. Given that these lunar rocks have Zr abundances of about 200-1800 ppm, zircon would have saturated at ~1100°C after >99.9% whole-rock crystallization. This precludes zircon crystallization as a significant influence on the trace-element evolution of lunar magmas.

In zircon-undersaturated melts, zircon xenocrysts will dissolve. The kinetics of dissolution have been determined experimentally in "granitic" melts of variable water content (Harrison and

Watson 1983) and in halogen-bearing hydrous "granitic" melts (Keppler 1993, Baker et al. 2002). Watson (1996a) modeled the dissolution of zircon in anatectic melts as a function of melt composition, water content and temperature, and concluded that only the largest crystals (>50-100 μm) would survive crustal fusion and incorporation into a >2 wt % H_2O, 750-850°C, zircon-undersaturated melt. A 50-μm diameter zircon would dissolve geologically instantaneously in an undersaturated, water-bearing granite (Harrison and Watson 1983). The presence of halogens up to ~1.5 wt % in the melt appears to have little affect on zircon dissolution kinetics or on Zr diffusion in the melt once zircon is dissolved (Baker et al. 2002). This may relate to the observation that in synthetic glasses Zr–F complexation does not occur (Farges 1996).

For some rock-types, such as intermediate S-type granites, it is common to observe multiple dissolution textures preserved within zircon crystals indicating periods of zircon-undersaturation followed by zircon-saturation in the melt (e.g., Vavra 1994, de la Rosa et al. 2002, Zeck and Williams 2002). Such crystals preserve compositional information for the melt prior to and after dissolution and may, therefore, record a change in composition relatable to an event such as magma-mixing.

Grain-size and external morphology. Typical igneous zircon is between 20 and 250 μm in the longest dimension with subhedral to euhedral face development. Larger mm-sized rare crystals are reported in kimberlites and kimberlite-related rocks (MARID-suite xenoliths); these are usually anhedral but can be subhedral (Kresten et al. 1975, Belousova et al. 1998, Hoskin 1998, Konzett et al. 1998). Large cm-sized colorless "gem-quality" crystals are found in the Mud Tank carbonatite (Hanchar and Hoskin 1998) although brown-colored imperfect crystals up to 30 cm-long from this carbonatite are displayed at the Australian Museum in Sydney. Large, sometimes mm-sized, red-colored zircons are reported from syenitic xenoliths in basalt, often associated with sapphire (Sutherland et al. 1998, 2002; Guo et al. 1996, Upton et al. 1999). In a general sense, form development and grain-size are dependent upon when zircon saturated in the crystallization history of a rock. Small, often acicular crystals, may have formed due to local saturation at the edge of an early-crystallizing phase (Bacon 1989), whereas early zircon-saturated melts tend to produce euhedral, larger crystals with width-to-length ratios of about 1:2-1:4. Late-crystallizing zircon in plutonic rocks tend to be anhedral because they have grown in the interstices between earlier-formed crystals (Scoates and Chamberlain 1995). Rapidly crystallized zircon in volcanic rocks is characterized by large width-to-length ratios (up to about 1:12) producing prismatic to acicular habits. Volcanic zircon, and sometimes plutonic zircon, can contain melt-trails that may be as long as the crystal itself (Chiarenzelli and McLelland 1993, Bussy and Cadoppi 1996).

Zircon has a highly variable external morphology. Often crystals are faceted with combinations of prism ({100} and {110}) and pyramid forms ({211}, {101} and {301}). Since the 1950s there have been attempts to systematically relate zircon morphology to petrogenesis (Poldervaart 1955, 1956; Larsen and Poldervaart 1957, Pupin and Turco 1972a,b,c; Kostov 1973, Hoffmann 1981). A typologic scheme relating the relative development of crystal forms with temperature and host-rock type was published by Pupin (1980) (the principal figure of that paper was reproduced as Fig. 9 in Speer 1982). Although this scheme was initially widely accepted and is still used (e.g., Dabard et al. 1996), three subsequent and ongoing observations have seen it rarely used: (1) zircon from a single rock and single age population can have widely varying morphologies; (2) zircon from widely different rock-types can have similar to identical morphologies with no systematic measurable differences despite claims to the contrary (see Fig. 9a of Wang et al. 2002); and (3) the external morphology of a single crystal can change a number of times during a single growth event (Fig. 2a) as a result of kinetic factors, such as diffusion rates and adsorption, which effect the growth-rates of crystal faces and therefore control the morphology of a growing crystal (Dowty 1980, Vavra 1990, 1993).

Internal textures. A large number of internal textures are now described for igneous zircon as a result of the application of CL and BSE imaging (e.g., Ono 1976, Paterson et al. 1989, 1992; Vavra 1990, Koschek 1993, Hanchar and Miller 1993, Corfu et al., this volume). These techniques are

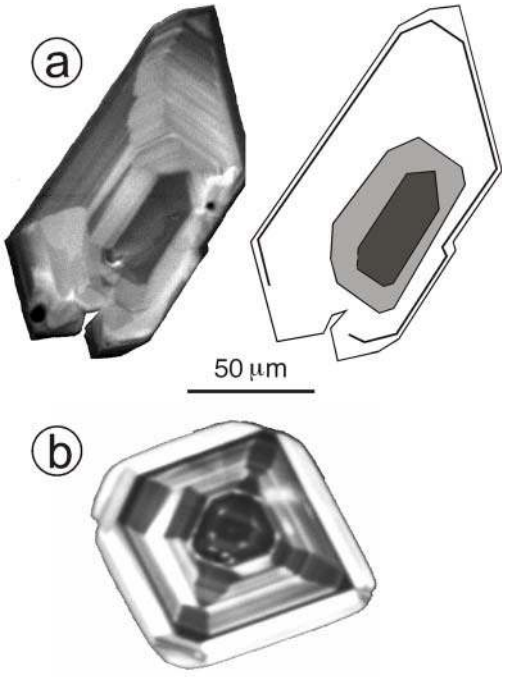

Figure 2. (a) *top row:* cathodoluminescence image (left) of zircon from an adamellite revealing changes in the external morphology (represented schematically, right) of the crystal during growth. After Hoskin (2000). (b) *bottom row:* cathodoluminescence image of zircon from an intermediate alkali volcanic rock, northeast Turkey. Both crystals exhibit well developed oscillatory and sector zoning as a result of heterogeneous trace-element distribution.

applicable because of the heterogeneous distribution of elements in most zircon, particularly trace elements. Oscillatory zoning, sometimes called growth zoning, occurs in many minerals (Shore and Fowler 1996) and is the predominant texture of igneous zircon. Early workers considered oscillatory zoning to be evidence that zircon crystallized over a long time period in a cooling magma (e.g., Silver and Deutsch 1963, Köhler 1970), yet saturation calculations and the inability to match zoning profiles (stratigraphy) from crystal to crystal reveals that this is likely to not be true for many zircon populations. Vavra, in the first of three classic studies (1990, 1993, 1994), used CL images of oscillatory zoning patterns (OZPs) of oriented crystal sections and related the OZPs to the relative growth velocities of crystal faces by delineating the boundary between different growth sectors (the delineated sector boundaries were called "Gratbahnen" or *ridge paths* in English). It was concluded that widely spaced OZPs, interrupted by surfaces of dissolution, represent a low degree of zircon-saturation in the melt and narrowly-spaced uninterrupted OZPs represent higher degrees of zircon-saturation (supersaturation). A method to quantify the growth-rate information of OZPs was developed in the second study (Vavra 1993), where the growth-rates of individual crystal faces were normalized to a reference face and plotted as a function of distance from a central point (representing zero time). Application of this quantification method to granitoid zircon indicated that the influence on the growth-rate of different forms can be attributed to either the degree of zircon-saturation or the incorporation of trace-elements (Vavra 1994).

Zircon OZPs have also been quantified by fractal statistics. Quantification in this way uses gray-scale data from CL images although derivation of statistical parameters varies (spectral analysis and Fourier transform, the width method, wavelet analysis). Halden and Hawthorne (1993) calculated the fractal dimension and Hurst exponent (H) of the OZP of a carbonatite zircon, finding H

to be in the range 0.34-0.42. Mathematically, this characterizes the OZP as "antipersistent," meaning that during crystal growth the growth-surface has a tendency to accept CL-emitting elements (the rare-earth elements, REE; Remond et al. 1992, Hanchar and Rudnick 1995) and then reject them: Halden et al. (1993) showed for the same crystal, that the oscillatory zoning correlated with significant variations in trace-element abundances. Hoskin (2000) and Fowler et al. (2002) also determined antipersistent *H* values; zircon from an I-type pluton in southeast Australia have *H* values averaging 0.44 (Hoskin 2000) and the large (~1.5 cm-long) zircon studied by Fowler et al. (2002) has *H* values ranging 0-0.11. The data of Fowler et al. (2002) fall outside of the *H* value range reported for other mineral species (0.25-0.45; Holten et al. 1997) possibly because the zircon megacryst formed from a brine and not a silicate melt (Fowler et al. 2002, p. 314).

The origin of oscillatory zoning in zircon probably involves a kinetic feedback mechanism operating at the crystal/melt interface. Evidence for processes operating at distance from that interface, even system-wide processes, is provided by large-scale harmonic zones that are broadly correlatable from crystal to crystal (Fowler et al. 2002) and the correlation between the Lyapounov exponent (λ), a fractal statistic, and NBO/T (Hoskin 2000). This correlation was interpreted by Hoskin (2000) to be due to ordering in the melt by polymerization. A data-constrained model was presented, where the oscillatory distribution of trace elements in zircon is controlled by dynamics at the zircon/melt interface involving cation substitution, diffusion, and melt polymerization and structure generation.

Sector zoning is also a dominant feature of igneous zircon. The texture is typical for volcanic zircon (Fig. 2b), but is also a common feature of plutonic zircon (Vavra 1990, Hanchar and Miller 1993, Benisek and Finger 1993) (Fig. 2a) despite slow growth-rates on the order of 10^{-19} to 10^{-15} cm/s and the expected attainment of equilibrium partitioning. Watson and Liang (1995) formulate a quantitative model for development of sector zoning in slowly grown crystals such as plutonic zircon (and metamorphic zircon). The model describes the disequilibrium uptake of trace elements as a function of crystal growth-rate and was applied in another study (Watson 1996b) specifically to zircon and surface enrichment of trace-elements during growth. Watson and Liang (1995) show that when surface enrichment occurs, trace-elements are entrapped by a relatively fast growing surface and that re-equilibration with the melt will not be achieved because the growth-rate is much faster than the sluggish intracrystalline elemental diffusivities (3+ cations, Cherniak et al. 1997a; 4+ cations, Cherniak et al. 1997b). These workers suggest that all zircon may be sector zoned and that we fail to detect all occurrences.

Major-element composition of igneous zircon

Zircon is zirconium orthosilicate, $ZrSiO_4$, and has a stoichiometric composition of 67.2 wt % ZrO_2 and 32.8 wt % SiO_2. The structure of zircon, as discussed by Finch and Hanchar (this volume), contains two cation sites; the 4-coordinated Si-site and the distorted 8-coordinated Zr-site. Both Si and Zr are tetravalent and have ionic radii of 0.84 Å and 0.26 Å, respectively. Although other minerals have a zircon-structure (e.g., xenotime, thorite and coffinite) none of these exhibit extensive solid solution with zircon, and only hafnon ($HfSiO_4$) and zircon have complete solid-solution (Ramakrishnan et al. 1969, Hoskin and Rodgers 1996). The extent of this solid solution in natural zircon is typically restricted although variation of the Zr/Hf ratio in zircon away from the chondritic value of ~37 is common. A compilation of published Hf values in zircon up to 1969 by Ahrens and Erlank (1969) showed a range in HfO_2 values from ~0.7-8.3 wt % with a mean of 2.0 wt %. Large variation above and below this 1969 mean value has now been reported as shown by the following examples (all values given here are wt % HfO_2): meteoritic zircon, 1.08-1.45% (Ireland and Wlotzka 1992); lunar zircon, 1.18% average (Wopenka et al. 1996); carbonatite zircon, Finland, 0.98% (Halden et al. 1993); diorite, China, ~1-3% (Wang et al. 2002) and from Chile, up to 1.65% (Ballard et al. 2002); granodiorite zircon, Chile, as low as 0.15% (Ballard et al. 2002); granite zircon, California, 1.78-3.17% (Wark and Miller 1993) and from the Czech Republic, up to 12.3% (Uher et al. 1998);

rhyolite zircon, Bishop Tuff, 1.04-1.29%; aplitic zircon, California, 5.17% (Wark and Miller 1993); granitic pegmatite zircon, Slovakia, 1-22% (Uher and Cerny 1998) and from Brazil, 0.89-0.95% (Halden et al. 1993); syenite zircon, Canada, 0.74-1.05%. The differentiation of Zr and Hf can be so pronounced as to produce zirconian-hafnon and hafnon (Correria Neves et al. 1974) and Zr/Hf ratios ranging 0.03-0.08.

Hoskin et al. (2000) analyzed zircon from all compositional zones within a zoned I-type pluton. The HfO_2 abundance in these zircon range 0.39-3.98 wt % (only 5 of 45 analyses are >3 wt %) and the mean of 2.4 wt % is close to the 2.0 wt % mean of Ahrens and Erlank (1969). These data and those of Hoskin and Ireland (2000) were suggested by Belousova et al. (2002) to be inaccurate on the basis of a comparison with only four other published studies and a selected set of data from Hoskin et al. (2000) and Hoskin and Ireland (2000). It was claimed by Belousova et al. (2002) that these HfO_2 values are "…generally much higher than those reported by other studies." (p. 618). This claim is not valid and is unsupported by a survey of the literature and even their own data. For example, Belousova et al. (2002) and Guo et al. (1996) report HfO_2 values for nepheline-syenite zircon up to 3.3 wt %, granitoid zircon up to 3.6 wt % and zircon inclusions in corundum up to 3.8 wt %.

Given that the most Hf-enriched zircon occur in evolved rock-types, it appears that the Hf abundance of zircon increases with magmatic differentiation. In a broad sense, this is observed for intrusive rocks from the McMurry Meadow pluton, California (Sawka 1988), the Sweetwater Wash pluton, California (Wark and Miller 1993) (Fig. 3), and the Boggy Plain Zoned Pluton, Australia (Hoskin et al. 2000). The fractionation of Zr and Hf in zircon-crystallizing melts was shown experimentally by Linnen and Keppler (2002) to be related to the Zr/Hf activity coefficient ratio in the melt, such that fractional crystallization of metaluminous and peraluminous granitic melts will decrease the Zr/Hf ratio of the residual melt and increase the abundance of HfO_2 in zircon.

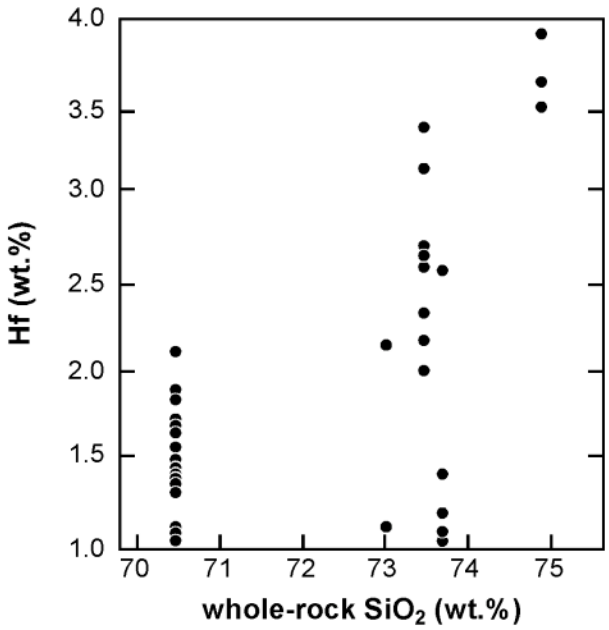

Figure 3. Hafnium (wt %) variation in zircon populations from the Sweetwater Wash pluton, southeastern California, U.S.A. Each data point is an analysis of a single crystal, or the mean of multiple analyses on a single crystal. Columns of data points represent the spread of Hf abundance in a single zircon population. Data from Wark and Miller (1993).

Trace-element composition of igneous zircon

A large number (~20-25) of trace elements are reported for zircon from *in situ* microprobe analyses (electron, laser, ion and proton beam techniques). In addition to Hf and Y (which for some zircon can be considered a minor-element, $0.1 < Y$ (wt %) < 1.0) the elements in greatest abundance are the rare-earth elements (REE), P, U and Th. Elements are substituted into zircon either by simple or coupled substitution mechanisms (general form: element = substituted element, where " = " means *substitutes for*):

Simple substitution mechanisms:

$Hf^{4+} = Zr^{4+}$		(i)
$(U^{4+}, Th^{4+}, Ti^{4+}, Sn^{4+}) = Zr^{4+}$		(ii)
$(OH)_4 = SiO_4$	Frondel (1953)	(iii)

Coupled substitution mechanisms:

(A) *At one site structural site:*

$(Y,REE)^{3+} + (Nb,Ta)^{5+} = 2\ Zr^{4+}$	Es'kova (1959)	(iv)

(B) *At two structural sites:*

$(Y,REE)^{3+} + P^{5+} = Zr^{4+} + Si^{4+}$	Speer (1982)	(v)
$Sc^{3+} + P^{5+} = Zr^{4+} + Si^{4+}$	Halden et al. (1993)	(vi)
$M^{n+} + n(OH)^{-} + (4–n)H_2O = Zr^{4+} + (SiO_4)^{4-}$	Caruba and Iacconi (1983)	(vii)

where M is a metal cation and n is an integer.

(C) *At an interstitial site:*

$(Mg,Fe)^{2+}_{(int)} + 3\ (Y,REE)^{3+} + P^{5+} = 3\ Zr^{4+} + Si^{4+}$	Hoskin et al. (2000)	(viii)
$(Al,Fe)^{3+}_{(int)} + 4\ (Y,REE)^{3+} + P^{5+} = 4\ Zr^{4+} + Si^{4+}$	Hoskin et al. (2000)	(ix)

The dominant mechanism for trace-element substitution in zircon is the "xenotime" substitution mechanism (mechanism v, above). However, the common occurrence of REE (mol %) in excess of P (mol %) in natural zircon, and also synthetic zircon, indicates that other mechanisms also operate (Romans et al. 1975, Speer 1982, Hinton and Upton 1991, Hanchar et al. 2001). Hoskin et al. (2000) argued that interstitial Mg^{2+}, Fe^{2+}, Fe^{3+}, and Al^{3+} in particular, could easily provide charge-balance for REE substitution greater than that allowed for by P substitution. They suggested two "xenotime-type" mechanisms (mechanisms viii and ix, above) and calculated that for their zircon an average abundance of only 380 ppm interstitial Al is required to provide charge-balance. A similar mechanism involving interstitial Li or Mo may have operated to charge-balance the REE-doped synthetic zircon of Hanchar et al. (2001). Other possible mechanisms for REE substitution include coupling with pentavalent Nb and Ta (mechanism iv, above) or by protonation of O^{2-} ions of $(SiO_4)^{4-}$ groups. The incorporation of water and hydroxyl into zircon is possible by mechanism (vii) although hydroxyl groups are probably the only hydrous species incorporated into igneous zircon during crystallization (Nasdala et al. 2001). Electrostatic neutrality could be maintained by O^{2-} vacancies, although static O-site vacancies are energetically unfavorable (Crocombette 1999, Williford et al. 1999) and are unlikely to persist in the zircon structure.

REE and Y abundance of igneous zircon. In the following discussions the REE will be grouped as follows: light REE (LREE), La–Pr; middle REE (MREE), Nd–Gd; and heavy REE (HREE), Tb–Lu. All ionic radii are from Shannon (1976). The 0.84-Å radius of the $^{[8]}Zr^{4+}$ ion is most closely matched by the smaller-radii HREE (e.g., $^{[8]}Lu^{3+}$, 0.977 Å) than the larger LREE (e.g., $^{[8]}La^{3+}$, 1.160 Å) such that the trivalent LREE are generally incompatible in the zircon structure. The absolute abundances of the LREE in igneous zircon are sub-ppm to ppm-level. This generality does not hold

for the element Ce which can be both trivalent and tetravalent; $^{[8]}Ce^{4+}$ has an ionic radius of 0.97 Å, close to Lu, and like the HREE, Ce is abundant in zircon. Hoskin (1998) reported Ce abundances in zircon from MARID xenoliths from South Africa, range 3 to 160 ppm, which almost span the range of Ce abundances reported for all other zircon occurrences (e.g., Hinton and Upton 1991, Barbey et al. 1995, Guo et al. 1996, Hoskin et al. 2000, Poller et al. 2001, Ballard et al. 2002, de la Rosa et al. 2002, Sano et al. 2002). Most analyses of igneous zircon report Ce abundances less than about 50 ppm. Where the abundance is significantly greater there is usually some question as to the provenance of the zircon, e.g., an inherited core (Griffin et al. 2002) or a metamorphic xenocryst (Hidaka et al. 2002). Cerium abundances in lunar and meteoritic zircon are characteristically very low (<1-7 ppm; Hinton and Meyer 1991, Ireland and Wlotzka 1992, Snyder et al. 1993, Wopenka et al. 1996).

In rocks with mantle affinity, zircon has a characteristically low total REE abundance. Belousova et al. (1998) in a study of kimberlitic zircon from southern Africa, documents total REE abundances (ΣREE) of about 5-39 ppm and Y in the range 11-74 ppm (Table 1). Hoskin and Ireland (2000) analyzed zircon megacrysts from the Jwaneng kimberlite which have ΣREE up to 12 ppm and Y up to 23 ppm. MARID suite zircon is relatively more enriched with ΣREE averaging 640 ppm and Y 895 ppm. Carbonatite zircons also have generally low ΣREE and Y abundances (Table 1). Zircon from crustal rocks have highly variable ΣREE abundances that vary from as low as ~250 ppm to as high as 5000 ppm and typically contain an average between 1500 and 2000 ppm. The abundances for zircon from the Syros ophiolite and Blind Gabbro, Australia, are relatively high and may relate to late-stage zircon saturation and growth in interstitial melt-pools that were highly enriched in the REE. Yttrium abundances vary similarly in crustal zircon and range from tens-of-ppm up to ~5000 ppm. Zircon associated with corundum-bearing xenoliths can be very enriched and contain ΣREE + Y up to 1.3 wt % (Guo et al. 1996; Table 1). These represent some of the most enriched, albeit rather uncommon, igneous zircon analyzed by *in situ* techniques. Generally, zircon contain less than 1 wt % ΣREE + Y and analyses containing significantly higher abundances almost certainly represent altered zircon or accidental analysis of inclusions.

A characteristic feature of most zircon is large intra-grain and inter-grain population compositional variation. Inter-grain order-of-magnitude variation of U and Th has long been observed during isotopic analysis of zircon populations (e.g., Black et al. 1986, Chen and Williams 1990) and large variations are also typically observed for the REE and Y. For example, plagiogranite zircon

Table 1. Rare-earth element and Y abundances of igneous zircon.

Lithology, rock name, source	ΣREE (ppm)	Y (ppm)	Reference
Vaca Muerta mesosiderite	10-719	-	Ireland & Wlotzka (1992)
Lunar, granite	1724	-	Hinton & Meyer (1991)
Lunar, granite breccia	735-1105	-	Snyder et al. (1993)
Lunar, monzodiorite breccia	464-1404	776-2660	Wopenka et al. (1996)
Kimberlite	5-39	11-74	Belousova et al. (1998)
	up to12	up to 23	Hoskin (1998)
MARID suite	640 av.	895 av.	Hoskin (1998)
Mud Tank carbonatite	26 av.	43 av.	Hoskin (1998)
Phalaborwa carbonatite	260	1000	Hoskin & Ireland (2000)
Silinjarvi carbonatite	~11	-	Halden et al. (1993)
Syros ophiolite	2952 av.	4437 av.	Hoskin & Ireland (2000)
Blind Gabbro	2780 av.	5184 av.	Hoskin & Ireland (2000)
Mawson igneous charnockite	986 av.	1497 av.	Hoskin & Ireland (2000)
Chilean diorites-granodiorites	~1500	up to ~4000	Ballard et al. (2002)
SE Australian diorite-aplite	250-3232	996-5514	Hoskin et al. (2000)
Torihama dacite	1180	-	Sano et al. (2002)
Manaslu granite and leucosomes	up to ~4000	up to ~4000	Barbey et al. (1995)
Carpathian granitoids	340-4205	up to ~5000	Poller et al. (2001)
Manila plagiogranite	1216 av.	1615 av.	Hoskin & Ireland (2000)
Anorthoclase-rich xenolith	up to 1813	up to 2455	Hinton & Upton (1991)
Corundum-bearing syenite	3505	4194	Hinton & Upton (1991)
Inclusions in corundum	383-5011	up to 8456	Guo et al. (1996)
Inclusions in corundum, Laos	3321-5785	3966-6275	Sutherland et al. (2002)

av. = mean value of multiple analyses.

from eastern Australia has Y abundances ranging from 399 to 3506 ppm (Hoskin and Ireland 2000) and Himalayan granitic leucosome zircon (sample MB301L) has Yb values ranging from 409 to 2215 ppm (Barbey et al. 1995). Poller et al. (2001) measured Y abundances in granitoid zircon (sample 1053 excluding cores) ranging from 500 to 4534 ppm and also reported near order-of-magnitude variation of REE and Y within an oscillatory zoned region of a single crystal (crystal 1032-8; analysis 1: ΣREE 328 ppm, Y 442 ppm; analysis 2: ΣREE 2830 ppm, Y 3420 ppm).

Inter-laboratory and inter-technique data-quality monitoring has been facilitated by the introduction of an internationally-available zircon REE standard called 91500 (Wiedenbeck et al. 1995). The standard contains about 300 ppm of REE + Y. Pieces of the standard are derived from an originally large megacryst from Ontario, Canada, although its original lithology is uncertain (*op. cit.*, p. 2). Published REE analyses of 91500 chips are few at present, although there is reasonable agreement between analyses from different laboratories using different techniques and data-treatment procedures (Table 2) such that 91500 should continue to be used as a primary or secondary standard.

REE patterns of igneous zircon. Zircon REE abundances are typically normalized to C1-chondrite values (e.g., McDonough and Sun 1995) and plotted on $\log_{10}$ versus element (La–Lu) diagrams (Fig. 4). Relative to chondrite values, lunar and terrestrial zircon are HREE enriched and LREE depleted. The normalized pattern is characterized by a steeply-rising slope from the LREE to the HREE with a positive Ce-anomaly and negative Eu-anomaly (Figs 4d-g, i, j). This style of pattern is characteristic for unaltered igneous zircon. Normalized element ratios are a measure of the steepness of the REE pattern; the greater the $(Sm/La)_N$ ratio, the steeper the LREE portion of the pattern and the greater the $(Lu/Gd)_N$ ratio, the steeper the HREE portion of the pattern (refer Fig. 4 with Table 3). These ratios are limited, however, and do not measure potentially useful petrogenetic information such as the degree of curvature in the HREE pattern of some zircon populations (Fig. 4e; both populations have $(Lu/Gd)_N$ ratios of 44, yet have different HREE concavity).

Compared with chondritic abundances, most zircon have LREE abundances typically less than $10^1\times$ chondrite, La usually much lower, although Ce is characteristically between 10^1 and $10^2\times$ chondrite. The MREE range from $10^0\times$ to $10^2\times$ chondrite and the HREE typically range between $10^3\times$ and $10^4\times$ chondrite (Fig. 4).

The abundance of Zr in meteorites ranges <4 ppm (chondrites) to 70 ppm (eucrites) and zircon has only been reported for a few occurrences. Ireland and Wlotzka (1992) were first to report *in situ* analyzed REE abundances and patterns of zircon from two meteorites, the Vaca Muerta mesosiderite

Table 2. Rare-earth element and Y composition of standard zircon 91500 (ppm ±1σ)*.

Element	Wiedenbeck[1]	Nesbitt[2]	Hoskin[3]	Belousova[4]	Sano[5]
n	1-6	10	17†	4	5-6**
Y			160 ± 23	147 ± 22	
La		0.003	0.04 ± 0.03		0.01 ± 0.01
Ce	2.0 ± 0.1	2.14	2.5 ± 0.2	2.5 ± 0.5	2.6 ± 0.4
Pr		0.01	0.03 ± 0.02		0.04 ± 0.02
Nd	0.4	0.25	0.3 ± 0.1		0.30 ± 0.06
Sm	0.3	0.50	0.4 ± 0.1	0.4 ± 0.2	0.28 ± 0.08
Eu	0.26 ± 0.07	0.23	0.22 ± 0.01	0.4 ± 0.2	0.19 ± 0.07
Gd	1.9 ± 0.1	2.38	2.0 ± 0.4	2.1 ± 0.4	1.6 ± 0.4
Tb		0.83	0.86 ± 0.06		0.8 ± 0.2
Dy	8.0 ± 0.1	10.8	11.03 ± 0.06	12 ± 2	12 ± 3
Ho		4.4	4.8 ± 0.3	4.9 ± 0.7	5 ± 1
Er	20.4 ± 0.8	24.2	25 ± 2	26 ± 4	29 ± 6
Tm		6.4	6.6 ± 0.4		8 ± 2
Yb	57 ± 17	69.7	65 ± 2	66 ± 7	77 ± 18
Lu	12.4 ± 0.9	12.6	13 ± 2	14 ± 2	17 ± 4
ΣREE	103+	134	132	128+	154

* A blank entry denotes element not analyzed for or below the limit of detection.
** Uncertainty is given as ± 2σ; *n* = the number of analyses contributing to mean REE and Y values.
† Includes SIMS and LA-ICP-MS data.
1. Weidenbeck et al. (1995); 2. Nesbitt et al. (1997); 3. Hoskin (1998); 4. Belousova et al. (2002); 5. Sano et al. (2002).

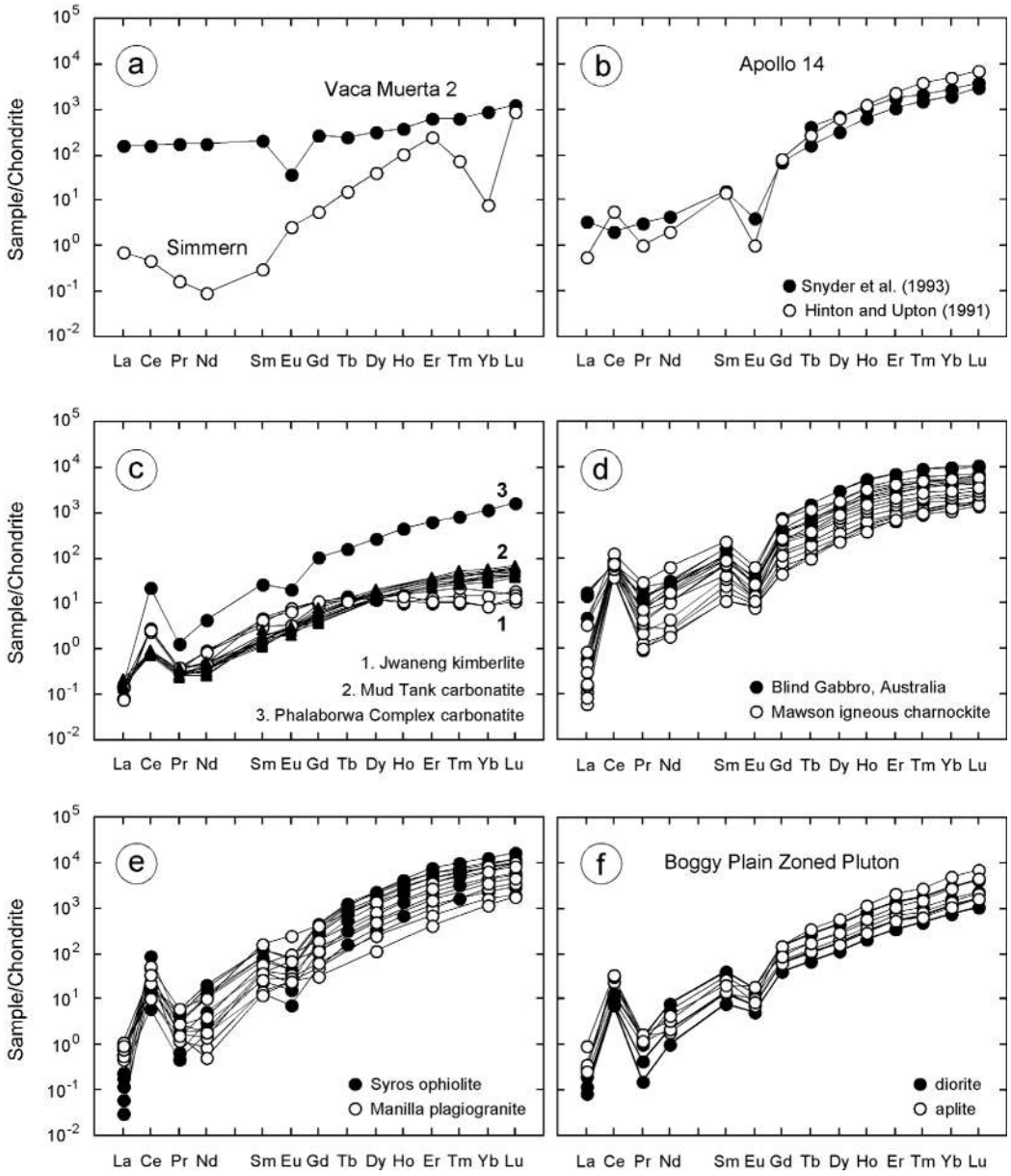

Figure 4. Compilation of REE patterns for meteorite, lunar and terrestrial zircon. (a) meteorite zircon from the Vaca Muerta mesosiderite and the H5 chondrite Simmern (Ireland and Wlotzka 1992); (b) lunar zircon from the Apollo 14 landing site (Hinton and Meyer 1991, Snyder et al. 1993); (c) kimberlite and carbonatite zircon (Hoskin and Ireland 2000); (d) zircon from Blind Gabbro, Australia, and Mawson igneous charnockite, Antarctica (Hoskin and Ireland 2000); (e) ophiolite and plagiogranite zircon (Hoskin and Ireland 2000); (f) zircon from two zones, diorite and aplite, of the Boggy Plain Zoned Pluton, BPZP (Hoskin et al. 2000); (g) Torihama dacite pumice, Japan (Sano et al. 2002); (h) zircon from sample NL102 of the Manaslu granite, Tibet (Barbey et al. 1995); (i and j) zircon from the Chuquicamata West porphyry and Los Picos diorite, Chile (Ballard et al. 2002); (k) zircon from corundum-bearing syenitic xenoliths, Elie Ness and Ilmen syentie (Hinton and Upton 1991); (l) Hadean zircon (4.0–4.15 Ga) from Jack Hills metaconglomerate W74, Australia (Peck et al. 2001). All data are replotted from the original source and normalized to the chondrite values of McDonough and Sun (1995).

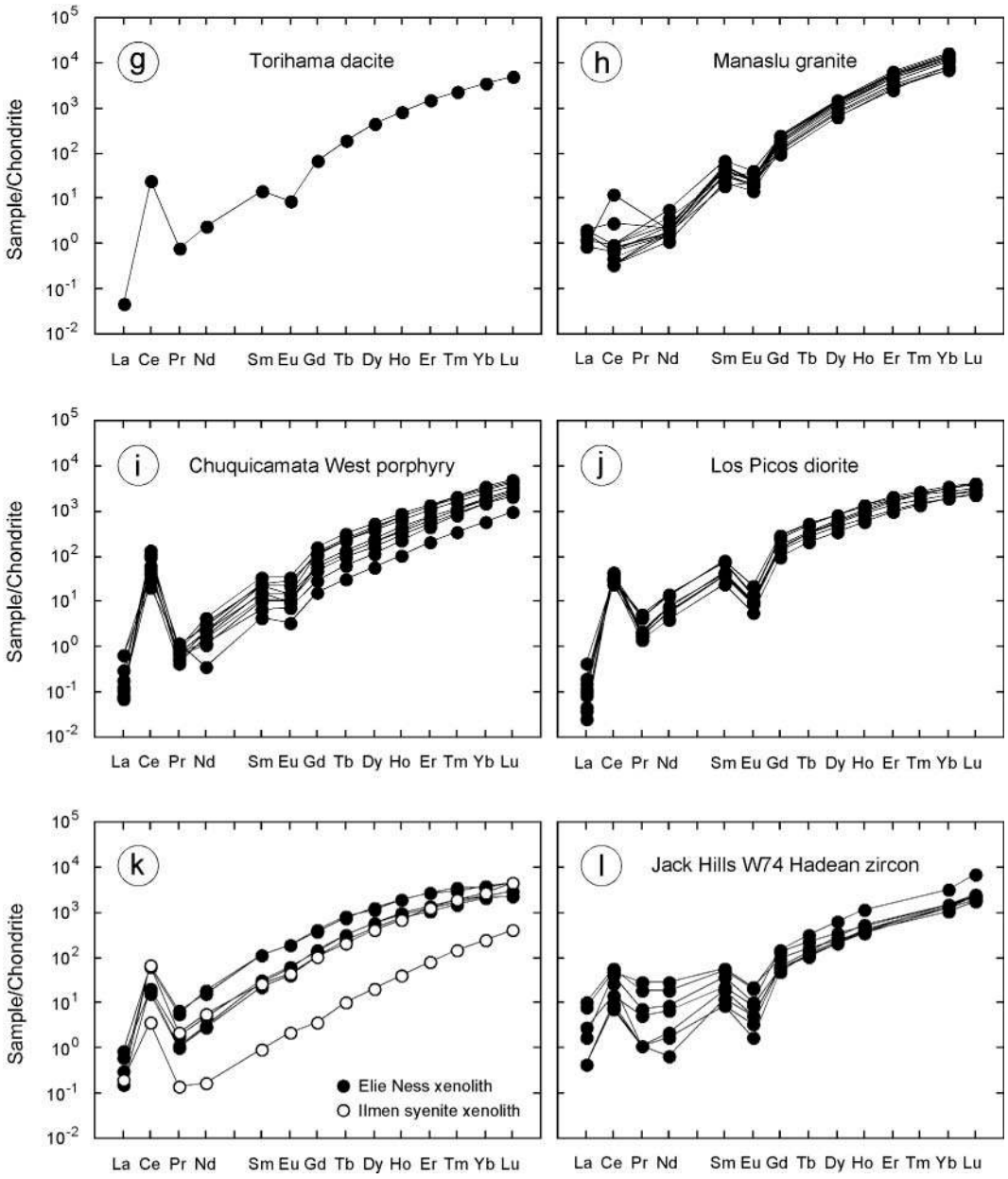

Figure 4.—Continued.

and the H5 chondrite Simmern. The REE pattern of zircon from Simmern (Fig. 4a and Vaca Muerta 1, not shown) is HREE enriched like unaltered terrestrial igneous zircon and apart from Tm and Yb, it increases regularly and steeply [$(Lu/Gd)_N$ = 169] from the MREE to the HREE. The similarity of the REE pattern to that of refractory inclusions in the Allende meteorite (Kornacki and Fegley 1986) indicates that the Simmern zircon pattern is an unusual mixture of igneous and volatility-influenced patterns. In contrast, Vaca Muerta zircon 2 formed very early in the evolution of the Solar System (at 4563±15 Ma) from an igneous melt. The REE pattern of this zircon is HREE enriched relative to the LREE, although the LREE are enriched (~10^3× chondrite) compared to

Table 3. Characteristic ratios of chondrite-normalized zircon REE patterns of Figure 4.†

Ratio**	Vaca Muerta zircon 2	Simmern	Lunar/ Apollo 14	Phalaborwa carbonatite	Mud Tank carbonatite	Jwaneng kimberlite
Figure 4	a	a	b	c	c	c
n	1	1	1	1	16	4
$(Sm/La)_N$	1.3	0.4	4.8	164	11.3	38
$(Lu/Gd)_N$	4.6	169	45	15	9.3	1.4
Ce/Ce*	0.9	1.3	0.6	49	3.7	13
Eu/Eu*	0.2	2.1	0.1	0.4	1.0	1.0
Ratio**	Blind Gabbro	Mawson ig. charnockite	Syros ophiolite	Manilla plagiogranite	BPZP diorite	BPZP aplite
Figure 4	d	d	e	e	f	f
n	8	10	8	7	7	4
$(Sm/La)_N$	153	236	547	90	119	57
$(Lu/Gd)_N$	16	19	44	44	27	38
Ce/Ce*	20	79	82	20	39	40
Eu/Eu*	0.2	0.2	0.3	0.9	0.2	0.3
Ratio**	Torihama dacite	Manaslu granite	Chuquicamata W. porphyry	Los Picos diorite	Elie Ness xenolith	Jack Hills zircon
Figure 4	g	h	i	j	k	l
n	6	13	10	9	6	8
$(Sm/La)_N$	306	33	145	653	165	18
$(Lu/Gd)_N$	74	-	47	19	17	35
Ce/Ce*	132	-	230	87	31	8.0
Eu/Eu*	0.3	0.3	0.4	0.1	0.9	0.2

† Chondrite normalizing values from McDonough and Sun (1995). Ce_N indicates the element has been normalized; $(Sm/La)_N$ indicates that the elements where normalized prior to division.
n = the number of analyses contributing to mean.

** Anomalies were calculated in this manner; for example $Ce/Ce^* = \frac{Ce_N}{\sqrt{La_N \cdot Pr_N}}$

unaltered terrestrial igneous zircon.

Lunar zircon have fairly steeply increasing patterns from the LREE ($10^1\times$ chondrite; $(Sm/La)_N = 4.8$) to the HREE ($10^2\times$ to $10^3\times$ chondrite; $(Lu/Gd)_N = 45$) and a pattern that, in general, is similar to terrestrial igneous zircon (Fig. 4b; see also Wopenka et al. 1996). A major difference, however, is that lunar zircon generally do not have a positive Ce-anomaly. The zircon described by Hinton and Meyer (1991) does have a Ce-anomaly but was found in an unusual oxidized granite that contains significant amounts of Fe_2O_3 and WO_3 (Meyer and Yang 1988).

A number of studies have shown that mantle-affinity zircon have REE patterns distinctively different from crustal-affinity zircon (Heaman et al. 1990, Belousova et al. 1998, Hoskin 1998, Hoskin and Ireland 2000). Zircon from kimberlite, MARID suite xenoliths (Hoskin 1998, Konzett et al. 1998) and the Mud Tank carbonatite (Currie et al. 1992, Hanchar and Hoskin 1998) (Fig. 4c) have HREE enriched patterns ($10^1\times$ to $10^2\times$ chondrite) with no significant Eu-anomaly ($Eu/Eu^* = 1.0$, i.e., no anomaly on average, Table 3) and relatively flat HREE patterns ($(Lu/Gd)_N \approx 1$-10). The exception to this is zircon from the Phalaborwa Complex carbonatite although its provenance may be silicic selvedges within the carbonatite (Hoskin and Ireland 2000, p. 629).

The REE patterns for continental crustal zircon populations from rock-types ranging igneous charnockite, gabbro, diorite, dacite, granite and aplite are given in Figures 4d-j. The patterns are generally similar with HREE abundances increasing from ~10^2 (Tb) to 10^4 (Lu) times chondrite, $(Sm/La)_N$ ranging 57-547 and $(Lu/Gd)_N$ ranging 16-74. The low $(Sm/La)_N$ value of 33 for Manaslu granite zircon is likely to be an artifact of analytical error because the patterns generally lack a positive-Ce anomaly which is observed for all other terrestrial zircon. Similarly, the very high $(Sm/La)_N$ value of 653 (Table 3) for Los Picos diorite zircon may be a result of underestimated La abundances.

Zircon from the Elie Ness and Ilmen syenite xenoliths are similar to other reported occurrences of corundum-associated zircon (Sutherland et al. 2002) in that they lack a negative Eu-anomaly, yet differ in this respect to other occurrences (Guo et al. 1996, Sutherland et al. 1998, 2002). Corundum-associated zircon tends to be more enriched than typical crustal zircon although the overall REE pattern (Fig. 4k) and normalized element ratios (Table 3) are not unusual.

Figure 4l is a series of REE patterns from early Archean (Hadean 4.0-4.15 Ga) zircon from Jack Hills metaconglomerate W74, Australia. These crystals are interpreted to have crystallized from an evolved granitic magma (Peck et al. 2001). Nearly identical REE patterns from the oldest recognized terrestrial mineral, zircon grain W74-2/36, also from Jack Hills, are likewise suggested to be of primary igneous origin, inherited from a silica-saturated granitic magma. These zircon crystals have been proposed to preserve evidence for a differentiated crust and liquid oceans on the very early Earth (Wilde et al. 2001, Valley et al. 2002). Zircon from W74 has a $(Lu/Gd)_N$ value (35) that falls within the range observed for zircon from continental crust rock-types (Table 3) although the $(Sm/La)_N$ value of 18 and Ce/Ce* value of 8.0 are most similar to mantle-affinity zircon ($(Sm/La)_N$ = 11.3-38, Ce/Ce* = 3.7-13). The Hadean zircons are LREE enriched. Abundances range from ~$10^{-1}\times$ to >$10^{1}\times$ chondrite. Peck et al. (2001) noted that these abundances are "…unusually high compared to REE concentrations…" (p. 4225) in typical crustal zircon, but noted that they "…are similar to LREE enrichment seen in late zircons from ~400-Ma aplitic rocks…" (p. 4225) from the Boggy Plain Zoned Pluton. Indeed this observation is correct, yet Wyborn (1983), Hoskin et al. (1998) and Hoskin (1999) demonstrated with textural, isotopic and trace-element data that those "late zircons" are most likely of a hydrothermal origin and did not crystallize from a magma. The observation of LREE enrichment in early Archean zircon cannot be used as evidence in support of a Hadean differentiated crust.

Ce and Eu anomalies of igneous zircon. Anomalous abundances of Ce or Eu, usually both, are a feature of all igneous zircon. Accurate and precise *in situ* data reveal that where anomalous abundances occur, the sense of the anomaly is always the same; Ce is always in greater abundance and Eu is depleted. Most zircons have both a positive Ce-anomaly and negative Eu-anomaly, but not all (e.g., Jwaneng kimberlite and Mud Tank carbonatite zircon, Fig. 4c; MARID suite zircon, Hoskin (1998), Fig. 5 therein). The magnitude of the anomalies are expressed as Ce/Ce* and Eu/Eu* ratios where Ce* and Eu* are the expected values for a smooth normalized pattern. These ratios are calculated according to the expression given in Table 3. Values of Ce/Ce* vary upward from 1.0 (lower values represent analytical artifacts or are in agreement with a value of 1.0 within analytical uncertainty) and Eu/Eu* varies between 1.0 (no anomaly) and zero.

Murali et al. (1983) first documented positive Ce-anomalies in zircon from Indian beach sands and a syenite and attributed it to the presence of Ce^{4+} in the crystallizing magma. Schreiber et al. (1980) suggested on the basis of Ce^{4+}/Ce^{3+}, Eu^{3+}/Eu^{2+} and Fe^{3+}/Fe^{2+} vs. fO_2 relations that Ce^{4+} cannot exist in magmas as it is reduced by Fe^{3+}, yet a small fraction of the Ce present can be tetravalent and on the basis of ionic charge and radius is compatible in zircon (Hinton and Upton 1991). Assuming equilibrium partitioning, the magnitude of the Ce-anomaly will be governed by the abundance of Ce^{4+} in the melt and this is related to the Ce^{4+}/Ce^{3+} ratio which is a function of oxygen fugacity. The small to non-existent Ce-anomalies in meteorite, lunar and mantle-affinity zircon (Fig. 4; Table 3) is consistent with their formation under reducing conditions and the "universal" and sometimes very large Ce-anomaly in crustal zircon is consistent with crystallization under variable yet relatively oxidized conditions.

Europium may exist in magmas as both a divalent and trivalent cation. The magnitude of the Eu-anomaly, like the Ce-anomaly, may be redox sensitive. If under oxidizing magma conditions all Eu is trivalent, the resulting normalized zircon REE pattern should not have a Eu-anomaly. However, under fO_2 conditions where Eu^{2+} is stable, a negative Eu-anomaly is expected because of the relative incompatibility of the large $^{[8]}Eu^{2+}$ ion (1.25 Å) relative to $^{[8]}Zr^{4+}$ (0.84 Å). Because all Eu should be trivalent under all conditions where Ce^{4+} is stable (Robie et al. 1979, Hanchar et al. 2001), a negative Eu-anomaly is not expected for crustal zircon. This consideration results in a paradox where the presence of a positive Ce-anomaly indicates oxidized magma conditions and a co-existing negative Eu-anomaly indicates reducing conditions. Previous discussion of this paradox lead Maas et al. (1992) to conclude that fO_2 is not the only factor controlling Ce^{4+}/Ce^{3+} and Eu^{3+}/Eu^{2+} in magmas.

This paradox may be explained by plagioclase fractionation which depletes Eu from the magma

prior to or during zircon crystallization (Snyder et al. 1993, Hoskin 1998, Hoskin et al. 2000). The Eu-anomaly in zircon, then, is both inherited from the Eu-depleted melt as well as being influenced by fO_2. This explanation may prove to only be one part of the paradox explanation and it may be that under some fO_2 and compositional conditions Eu^{2+} and Ce^{4+} can co-exist, or that redox reactions at the zircon/melt interface influence the oxidation state of Ce.

A systematic relation between zircon Ce and Eu-anomalies, the oxidation-state of a suite of host rocks and their age has been demonstrated for the first time by Ballard et al. (2002). In this study of zircon from barren and Cu-mineralized intrusive rocks from Chile, the Ce^{4+}/Ce^{3+} ratio was calculated using a lattice-strain model for zircon/melt partitioning of Ce^{3+} and Ce^{4+}. These workers found that Ce^{4+}/Ce^{3+} and Eu/Eu* ratios varied systematically in time and with compositional evolution of the intrusive suite. The greater variation was found for the Ce^{4+}/Ce^{3+} ratio (Fig. 5). In general, Ce^{4+}/Ce^{3+} and Eu/Eu* in the Chilean zircon—and by inference, magmatic oxidation-states—increased from older mafic host rocks to younger felsic rocks. For this suite of rocks, Cu-mineralization is associated with zircon populations having average Ce^{4+}/Ce^{3+} ratios >300 (i.e., Ce/Ce* >70) and Eu/Eu* >0.4 (e.g., the Chuquicamata West porphyry, Table 3). A similar temporal relation with Ce/Ce* and Eu/Eu* was observed for igneous zircon populations preserved in Palaeoproterozoic paragneisses in Japan, although the trend is opposite from that found by Ballard et al. (2002) and Ce/Ce* and Eu/Eu* ratios decrease over time (Hidaka et al. 2002). The authors do not offer an explanation for this apparent trend which becomes simple scatter when the anomalies are recalculated in the manner of those in Table 3.

Other trace-element occurrences in igneous zircon. The most studied trace elements in zircon are U, Th and Pb produced by radioactive decay (e.g., Ahrens 1965, Ahrens et al. 1967, Poller et al. 2001, hundreds of U-Th-Pb geochronology studies). While non-radiogenic Pb ($^{[8]}Pb^{2+}$ 1.29 Å) is largely excluded from a crystallizing zircon (Watson et al. 1997), Th and U are somewhat compatible (ionic radii: $^{[8]}Th^{4+}$ 1.05 Å, $^{[8]}U^{4+}$ 1.00 Å) and occur in crustal zircon with abundances typically ranging tens- to thousands-of-ppm. The lowest abundance of U and Th yet reported for zircon is for Vaca Muerta meteorite crystal 1 where U is 0.58 ppm and Th is 0.051 ppm (Ireland and Wlotzka 1992). The intracrystalline distribution of Th and U in igneous zircon is heterogeneous and even varies about 35% (2σ) in the 91500 zircon standard (Belousova et al. 2002). Despite such variation on a ~30-50 µm scale, the Th/U ratio varies much less as pointed out by Ahrens (1965) and confirmed many times since. Generally, the Th/U ratio of igneous zircon is ≥0.5. Clear exceptions to this are zircon from less common rock-types such as kimberlite and MARID suite xenoliths

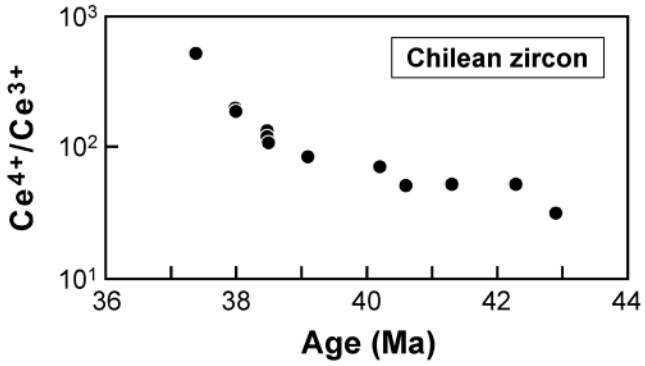

Figure 5. Average Ce^{4+}/Ce^{3+} ratios versus U-Pb age of zircon from the Los Picos-Fortuna/Pajonal-El Abra igneous complex and the El Abra mine porphyry, Chile. The Ce^{4+}/Ce^{3+} ratios increase systematically from the oldest, most mafic rocks, to the youngest, most felsic rocks, which are also Cu-mineralized. This relation is inferred to reflect a systematic oxidation increase of the magmas producing these rocks. Data from Ballard et al. (2003).

where Th/U values range ~0.2-1.0 (Konzett et al. 1998) and zircon from carbonatites from the Kola Peninsula, Russia, where Th/U ratios vary up to 9000 (Amelin and Zaitsev 2002).

Unaltered igneous zircon has very low concentrations of all other *in situ* measured elements. These elements include Li, Be, B, F, Na, Mg, Al, P, Ca, Sc, Ti, V, Cr, Mn, Fe, Sr, Nb, Ba and Ta. With the exception of P, the combined abundance of these elements in a single crystal is likely to be much less than a few hundred ppm and they are most often below the limit of detection. Values for these elements as given below (except P) should be considered as indicative of the upper ppm limits of abundance. Phosphorous values for zircon from the calc-alkaline intrusive suite of Ballard et al. (2002) range 49-388 ppm and for diorites through aplites of the Boggy Plain Zoned Pluton, zircon P values range 281-1379 ppm (Hoskin et al. 2000). For most of the crystals analyzed in these two studies, the mol % of P is not sufficient to charge-balance the mol % of REE indicating that the "xenotime" substitution mechanism must be only one of the operating REE substitution mechanisms. Niobium varies up to 62 ppm, Ta is <3, Li <3, Be <0.01, B <0.1, F <10, Na up to 28, Sc up to 250, Ti up to 75, V <5, Cr <0.5, Mn <40, Sr up to 6 and Ba <2 ppm (Hinton and Upton 1991, Maas et al. 1992, Halden et al. 1993, Hoskin et al. 2000, Ballard et al. 2002). The abundances of Mg, Al and Fe are highly variable and can be present at the hundreds-of-ppm level or below detection limits. Wopenka et al. (1996) reported an average Al_2O_3 value of 0.02 wt % and FeO of 0.10 wt % for lunar zircon, whereas Dickinson and Hess (1982) report up to 1.3 wt % Al_2O_3 in a lunar zircon. Guo et al. (1996) measured up to 0.54 wt % Al_2O_3 and 0.32 wt % Fe_2O_3 in corundum-associated zircon. Magnesium is less abundant (MgO <0.2 wt %; Dickinson and Hess 1982, Guo et al. 1996, Sutherland et al. 2002).

A number of trace-elements in zircon including the REE, where analyzed by Belousova et al. (2002), including Ti, Mn, Fe, Ga and Sn. However, their data-base includes analyses of supposed zircon containing MnO abundances up to 0.4 wt %, 0.5 wt % Nb_2O_5, 1.4 wt % UO_2, 2.9 wt % P_2O_5, 4.1 wt % TiO_2, and 6.0 wt % Fe_2O_3. These data cannot represent primary igneous zircon and reflect analysis of altered zircon or zircon + inclusions. Non-primary abundances of Fe_2O_3 like those of Belousova et al. (2002), as well as other oxides including elevated MnO, Al_2O_3 and CaO are reported for metamict and fluid-altered zircon (e.g., Kopchenova et al. 1974, Geisler and Schleicher 2000, Geisler et al. 2003).

Given the very low abundances of elements that may have a role in REE-coupled substitutions in addition to P (e.g., Nb, Ta), it seems that interstitial cations, Al^{3+} in particular (Hoskin et al. 2000), and perhaps hydrous species, play an essential role in REE and Y substitution.

Zircon composition and investigations of igneous processes

Zircon saturation, fractionation and melt composition. Due to the HREE enriched character of igneous zircon, saturation and fractionation of this phase during magmatic differentiation might cause significant depletion of the magma in the HREE. For this to be the case, however, relatively large amounts of zircon may be required. In a study of the distribution of REE among minerals in "Route 111" granodiorite from California, Gromet and Silver (1983) found that along with zircon, titanite, allanite and apatite were the main HREE phases. However, on the basis of compositional and modal analysis, the fractional contribution of zircon to the total whole-rock HREE abundance is almost insignificant. In the Route 111 granodiorite, most of the REE are hosted in titanite (MREE and HREE), allanite (LREE) and hornblende. In this case, during magma evolution, zircon could not have been expected to have exerted a noticeable influence on the HREE. This is also the case for granitoid samples from the Saganaga tonalite, Minnesota–Ontario, where despite the presence of zircon, apatite and titanite, the REE characteristics of the magmas seem to have been governed by petrogenetic processes operating prior to the saturation of these REE-bearing phases (Evans and Hanson 1993). Sawka (1988) also concluded that zircon did not influence the REE characteristics of magmas forming the McMurry Meadows Pluton, California, because zircon may have crystallized from the bulk (homogeneous) magma prior to differentiation.

Zircon fractionation has, however, been demonstrated for other igneous systems to be an important fractionator of the HREE, Y and Hf. Tertiary lavas ranging from basaltic andesite to high-silica rhyolite from the Batopilas area of Mexico were examined by Evans and Hanson (1993). The variation of Zr abundance in the Batopilas lavas strongly suggests zircon was an early-liquidus saturation phase in the high-silica rhyolite lavas. The inclusion of zircon in a model fractionating assemblage, improved an earlier modeling attempt (Cameron and Hanson 1982) to relate the high-silica rhyolites to less felsic dacites by bringing the REE modeling results into better agreement with the major-element modeling results. Because zircon is HREE enriched, only 0.06 wt % of zircon was required in the model assemblage to produce a better agreement. Another demonstration of the role of zircon during differentiation was given for granitoid rocks of a small I-type pluton in southeast Australia. The Boggy Plain Zoned Pluton (BPZP) contains a range of REE-bearing accessory phases including apatite, titanite, allanite, monazite and zircon. Hoskin et al. (2000) demonstrate an integrated approach to identifying the point at which these minerals saturate in the evolution of the magmatic system. Once a mineral saturation point is identified, and assuming fractionation, that mineral can be included in the model assemblage for numerical modeling of differentiation processes. Erroneous modeling results will occur if a mineral is included in the model assemblage prior to its saturation point and fractionation. Hoskin et al. (2000) modeled compositional variation within the adamellite zone of the BPZP by 90% fractional crystallization of an assemblage containing 22 wt % calcic-amphibole, 19 wt % alkali-feldspar, 37 wt % plagioclase, 17 wt % biotite, 4 wt % clinopyroxene, 0.13 wt % apatite, 0.1 wt % allanite and 0.19 wt % zircon. The difference between measured whole-rock REE abundances and modeled abundances is between 1 and 15% and the model reproduces the measured normalized REE pattern (Hoskin et al. 2000, Fig. 16 therein).

Melt-composition calculations. A number of studies have attempted to determine trace-element zircon/melt partition coefficients either by experiment or analytically (Nagasawa 1970, Watson 1980, Mahood and Hildreth 1983, Murali et al. 1983, Fujimaki 1986, Bea et al. 1994, Sano et al. 2002, Thomas et al. 2002, Thomas et al., this volume) or partly by theoretical considerations (Hinton and Upton 1991, Guo et al. 1996). These have been used in attempts to determine the composition of melts from which zircon has crystallized. Success of the application of partition coefficients, $^{\text{zircon/melt}}D_{\text{element}}$, for the back-calculation of melt composition is dependent upon high-quality trace-element data for zircon and well known D_{element} values, as well as the assumption that zircon crystallized early from the melt. If this last assumption is not justified, neither is the use of D_{element} values because the best of these values have been determined from known melt compositions and generally, the composition of a later-stage zircon-crystallizing melt is unconstrained, and D_{element} values vary strongly as a function of melt composition. It is likely that this is one reason why many workers have not been able to back-calculate melt compositions that look reasonably similar to any common melt or rock-type on Earth or the Moon (e.g., Hinton and Upton 1991, Snyder et al. 1993, Guo et al. 1996). Perhaps more important is the further assumption one must make when using D_{element} values, which is that equilibrium trace-element partitioning governs the abundance of trace-elements in zircon. It is suspected however, that disequilibrium partitioning is normal for zircon (Watson and Liang 1995, Barbey et al. 1995, Watson 1996b). Moreover, the partitioning of REE, Y and P into zircon appears to be limited not so much by melt composition or cation diffusion, but by intracrystalline strain imposed by cation substitution (Finch et al. 2001). Despite these real difficulties, the determination of D_{element} values by Sano et al. (2002) and Thomas et al. (2002) appear to be more realistic and able to reproduce known melt compositions (Sano et al. 2002, p. 227-228).

Provenance-indicator studies using igneous zircon composition

The chemical and mechanical durability of zircon means that it can persist on and within Earth's crust for billions of years. As well as preserving textural information and age data, a record of the source-rock composition of detrital or xenocrystic zircon may be preserved by trace-element abundances and patterns. It would be of immense interest in crustal evolution studies to be able to

"finger-print" source-rock lithology and age from detrital and xenocrystic zircon. The dual approach of assessing zircon isotope and trace-element composition would have potential in determining sediment provenance and its applications to studies of, for example, uplift, erosion and tectonics.

For the composition of *ex situ* zircon to be used to identify source lithology, it must be demonstrated that zircon composition can be systematically related to lithology. Such a demonstration could be via the use of partition coefficients, or by identifying compositional features of zircon that can be systematically related to lithology. The latter approach seems most promising and studies taking this approach are discussed here. Early studies relating zircon composition and isotopic age to source lithology were limited by the inability to measure or accurately determine REE, Y and other trace elements in zircon (Köppel and Grünenfelder 1971, Köppel and Sommerauer 1974, Murali et al. 1983). Using multi-grain INAA analysis of seventeen zircon populations, Heaman et al. (1990) proposed that zircon from kimberlite, carbonatite and nepheline syenite, mafic and ultramafic samples, felsic samples, and basalts could be distinguished from each other on the basis of plots of Lu, Sc, Th/U and Lu/Sm versus Hf. However, on the basis of Lu, Sc, Th/U and Lu/Sm alone, there is no clear discrimination, and only partial discrimination based on the reported Hf abundances. Nonetheless, this important paper indicated the potential for zircon composition as a provenance and petrogenetic indicator.

The first *in situ* measurements of zircon composition from a variety of rock-types, including meteorites, lunar rocks, metamorphic zircon and two granitoid zircons, were made by Ireland and Wlotzka (1991). Their nine REE analyses showed that despite the diverse geologic settings in which the terrestrial, lunar and meteoritic zircon formed, their REE patterns are remarkably similar. Interestingly, there is greater difference between the REE patterns of two zircons from a single meteorite than there is for all terrestrial zircon measured in their investigation. A much larger data set of REE, Y, P and HfO_2 was collected by Hoskin and Ireland (2000) for zircon from a wide-range of mantle-affinity and crustal rock-types. This study concluded that the REE abundances and patterns of zircon from rocks with a mantle-affinity are distinctive from crustal zircons and have much flatter patterns and lower abundances. This conclusion is supported by Belousova et al. (1998). Despite this difference in REE characteristics, no systematic difference between zircon from disparate crustal rock-types was observed.

To evaluate the actual variation in detrital zircon REE composition in a real sediment, zircon from a sandstone sample from the North Sea were analysed by Hoskin and Ireland (2000). The sandstone is from the Statfjord Formation (Zone A) and was sampled at 9877.5 ft (3.01 km) downhole of Brent Field well 211/29-6 located on the sea floor between Scotland and Norway. Evidence from Sm–Nd isotopes, palaeocurrent data, heavy mineral assemblages, detrital garnet composition, and detrital zircon U-Pb isotope spectra, indicate that the source region of this sample comprised high-grade metasediments and a range of Caledonian intrusive rocks. The REE abundances for zircon from this sandstone reveal that despite different crustal elements in the source region and a U-Pb zircon age range of 2.82 billion years, the zircon REE patterns are essentially identical. This result cannot be attributed to a homogeneous source region or derivation of detritus from a single source, but was considered by Hoskin and Ireland (2000) to confirm the apparent monotony of REE patterns and abundances in zircon derived from a range of common crustal rock-types.

Belousova et al. (2002) measured a large range of trace-elements in zircon from a variety of rock-types, but dominantly kimberlite, lamproite and carbonatite. This study and that of Hoskin and Ireland (2000) and Heaman et al. (1990) are summarized in Table 4. The value of the study by Belousova et al. (2002) is reduced because their data-base includes analyses of "metamict zircons…" that have compositions that have been affected by "…secondary alteration" (p. 609). Moreover, their supposed basalt zircon actually derive from xenoliths within the basalt, while other zircon are detrital and derived from a "palaeochannel" (p. 604) and the original source-rock(s) is unknown. Data from these zircon occurrences are included in statistical classification and regression trees

Table 4. Characteristics of zircon trace-element and provenance studies.

Heaman, Bowins and Crocket (1990) Geochim Cosmochim Acta 54:1597-1607

Strengths
• first analyses of zircon from a variety of widely sourced rock-types.
• demonstrated a degree of discrimination for zircon provenance on the basis of Hf (wt %).

Limitations
• very small data set of multi-grain analyses (INAA)

Hoskin and Ireland (2000) Geology 28:627-630

Strengths
• first high-quality *in situ* analyses of zircon from a variety of widely sourced rock-types.
• REE and Y data for well-constrained whole-rock samples, texture imaged and U-Pb isotope analyzed zircon from those whole-rock samples.
• provided a "real-life" test of zircon provenance identification on a well studied sandstone from the Statfjord Formation, North Sea.

Limitations
• limited data set

Belousova, Griffin, O'Reilly and Fisher (2002) Contrib Mineral Petrol 143:602-622

Strengths
• zircon analyses from a variety of widely sourced rock-types.
• data set of elements includes REE, Y and other trace-elements.

Limitations
• no documentation of intra-sample compositional variation or "representativeness".
• data set of rock-types includes some of uncertain origin or identification.
• data set of zircon compositions include analyses of altered zircon or zircon + inclusions.
• statistical determination of zircon source rock-type is based on the flawed data sets above.
• statistical treatment (CART tree) is a description of original data set and should not be used predictively.

(CART tree) that are intended to be used to identify the source rock-type of a detrital or xenocrystic igneous zircon. The CART trees are a "description" of the specific data set from which they are constructed such that the "description" is only as good as the data-base.

At this point in time, delineation and recognition of systematic relations between igneous zircon composition and source rock-type are only slowly emerging. Studies of metamorphic zircon, however, reveal that the composition provides a great deal of information about the processes that form metamorphic zircon and metamorphic rocks.

ZIRCON AND METAMORPHIC PETROGENESIS

Textural characterization of metamorphic zircon

Metamorphic zircon is characterized by a number of features that differ from igneous zircon and these are considered separately below. A more detailed review of metamorphic zircon textures is given by Corfu et al. (this volume).

External morphology of metamorphic zircon. Zircons in low-grade metamorphic rocks are usually inherited from the protolith and may show signs of resorption or metamorphic overgrowth. High-grade rocks such as granulites may contain zircon that grew during metamorphism in the presence or absence of an anatectic melt (Fraser et al. 1997, Roberts and Finger 1997). Typical morphologies are rounded or ovoid shapes (Fig. 6a) which are interpreted to be formed by resorption by a zircon-undersaturated intergranular fluid (Hoskin and Black 2000) which may also produce surface etching and pitting (Wayne and Sinha 1988, Hanchar and Miller 1993). Ovoid morphologies were also documented by Degeling et al. (2001) who proposed that new zircon formed during the decompression reaction of garnet + sillimanite + quartz to produce zircon-bearing cordierite. Rounded and ovoid zircons are often accompanied by "soccer-ball" shaped zircon (e.g., Vavra et al. 1996, Schaltegger et al. 1999; Fig. 6b). Soccer-ball zircon represents the S22-type in the Pupin (1980) morphology classification scheme, with subordinate development of prism faces. Hoskin

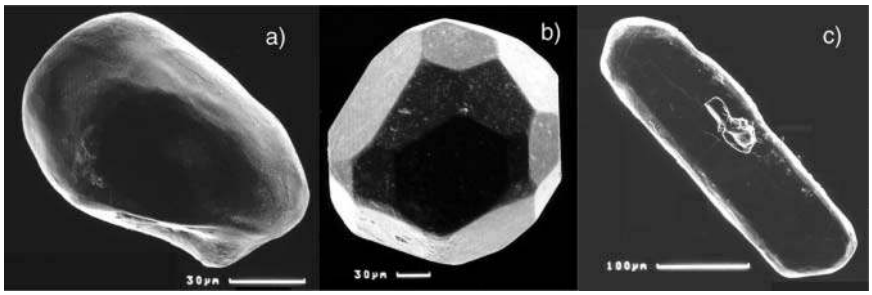

Figure 6. Zircon in granulite-grade rocks, Vosges Mountains, eastern France: (a) rounded-ovoid grain; (b) "soccer-ball" zircon; (c) prismatic zircon from the same granulite as the grain in (a), but occurring on the grain-boundaries of rock-forming minerals. Figure after Schaltegger et al. (1999).

and Black (2000) found that within their high-grade rocks, zircon included within different rock-forming minerals and those from grain-boundaries did not differ morphologically. However, it was reported by Schaltegger et al. (1999) that soccer-ball zircon included in ternary feldspars are coeval with prismatic grains that occur on grain-boundaries (Fig. 6c).

Internal textures of metamorphic zircon. Internal textures are observed by CL and BSE imaging (Hanchar and Rudnick 1995, Rubatto and Gebauer 2000, Kempe et al. 2000, Corfu et al., this volume). These images allow for visual distinction between metamorphic growth zones, preserved igneous cores, recrystallized domains and domains showing other types of structural reorganization. Zircon that grew in high-grade metamorphic rocks often shows a distinct sequence of internal structures: an initial low-luminescence growth zone (sometimes overgrowing an inherited core) sequentially overgrown by sector zoned domains. These textures are commonly followed by oscillatory zoned domains (Vavra et al. 1996, 1999; Schaltegger et al. 1999; Fig. 7). This succession of zones has yet to be adequately explained and has not yet been the subject of specific research attention.

Metamorphic zircon can preserve a wide variety of textures, largely because it can grow under a wide variety of *P-T-x*-stress conditions that may collectively be termed as metamorphic. Zircon-forming events may occur prior to, after, or at peak *P-T* conditions. The geologic significance of an isotopic age determined from a metamorphic zircon depends upon when in the petrogenesis of the rock the zircon (or a specific growth zone) formed, whether or not it formed in the solid-state, by precipitation from a fluid (carbonic, aqueous, or melt), or by recrystallization of protolith zircon. Given the complexity of zircon textures and the ambiguity associated with interpreting isotopic age determinations, trace-element analysis is becoming widely applied as another line of evidence for more confident petrogenetic interpretation.

The growth of new zircon during metamorphism and its composition

The crystallization of new zircon during metamorphism has been recorded for a wide range of temperatures and pressures during prograde (Liati and Gebauer 1999, Bingen et al. 2001), retrograde (Pan 1997, Roberts and Finger 1997, Degeling et al. 2001, Whitehouse and Platt 2003) and peak (Bea and Montero 1999, Hoskin and Black 2000, Möller et al. 2002) metamorphic conditions. At *P-T* conditions lower than upper-amphibolite and granulite-grade, new zircon is rare and recrystallization of protolith zircon is responsible for producing "metamorphic" zircon. At granulite-grade conditions, new zircon can form at sub-solidus conditions and also during anatexis (Schaltegger et al. 1999, Rubatto et al. 2001). The volume of new zircon formed is dependent upon temperature and the volume and composition of melt (Watson and Harrison 1983, Watson 1996a). There are examples, however, where the volume of new zircon exceeds-by-far that expected from calculated

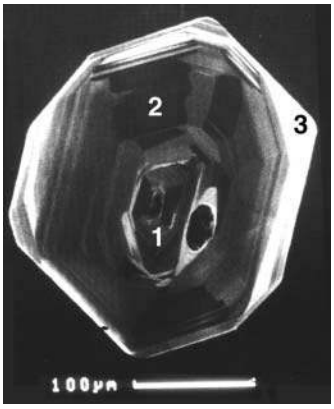

Figure 7. A metamorphic zircon illustrating the commonly observed sequence of growth structures: (1) low-luminescence center; (2) sector zoned domain; (3) oscillatory zoned outer part. The bright-CL area to the right of domain 1 is an area of localized recrystallization around a 40-µm mineral inclusion. Figure after Schaltegger et al. (1999).

saturation limits. Vavra et al. (1996, 1999) report that zircon in metasediments from the Ivrea Zone, southern European Alps, are comprised of 5 vol % of inherited zircon overgrown by large volumes of new zircon. They also describe voluminous overgrowths in associated melanosomes, which according to compositional criteria should not have been favorable to high Zr solubility and subsequent zircon growth. Other factors that determine whether new zircon will form or not include the grain-size of zircon and the crystal size-distribution of rock-forming minerals (Nemchin et al. 2001), the location of protolith zircon on grain-boundaries or as inclusions (Watson et al. 1989, Watt and Harley 1993), diffusion of Zr in a melt phase and the Zr abundance and stability of rock-forming minerals.

The Zr abundances of major metamorphic minerals in four different granulite-grade rocks from Rundvågshetta, east Antarctica, were determined by Fraser et al. (1997). Both garnet and hornblende contain tens of ppm of Zr, enough to produce new zircon by Zr release if these minerals partake in breakdown reactions such as garnet + sillimanite + quartz → cordierite + zircon. Vavra et al. (1996) had proposed that biotite was a source of Zr for new zircon growth during anatexis in the Ivrea Zone. Pan (1997) proposed zircon, titanite and rutile formation by breakdown of zirconolite, and zircon formation after allanite breakdown in upper-amphibolite grade gneisses. Ilmenite was proposed as a source of Zr for metamorphic zircon by Bingen et al. (2001). The formation of new zircon by these net-transfer reactions is, however, dependant upon the solubility of Zr in product phases. At Rogaland in southwest Norway, zircon formed in high-grade rocks by the reaction garnet + sillimanite + quartz → cordierite + zircon, but did not form during the reaction garnet + sillimanite + quartz + biotite → osumilite + orthopyroxene + spinel + magnetite, because of the higher solubility of Zr in osumilite and orthopyroxene at higher grades than in cordierite at lower grades (Degeling et al. 2001). Unfortunately, compositional data for zircon formed by net-transfer reactions are scarce, largely due to very small grain-sizes (typically <20 µm).

In a study of trace-element partitioning between co-existing zircon and garnet, Rubatto (2002) demonstrates that among the REE, Ce has by-far the highest preference for zircon ($^{Ce}D_{zir/gt}$ = 69-90; next largest is $^{Lu}D_{zir/gt}$ = 12-24) thus producing extremely large positive Ce anomalies in zircon that even exceed the chondrite-normalized Yb and Lu values (Fig. 8). The REE patterns of zircons that formed by net-transfer reactions in the high-grade rocks of Rubatto (2002) are additionally characterized by relatively depleted HREE abundances due to partitioning competition with garnet and very small (Eu/Eu* = 0.24-0.63) negative Eu anomalies which are believed to be "inherited" from the whole-rock composition as well as indicate formation in the absence of plagioclase. Nearly identical REE patterns were reported by Whitehouse and Platt (2003) for zircon rims on protolith cores included in metamorphic garnet, although these workers suggest that Ca-rich garnet rims and zircon rims grew from melt produced during decompressional melting. In addition to *P-T* indicator minerals that can be included in metamorphic zircon (e.g., Hermann et al. 2001, Katayama et al.

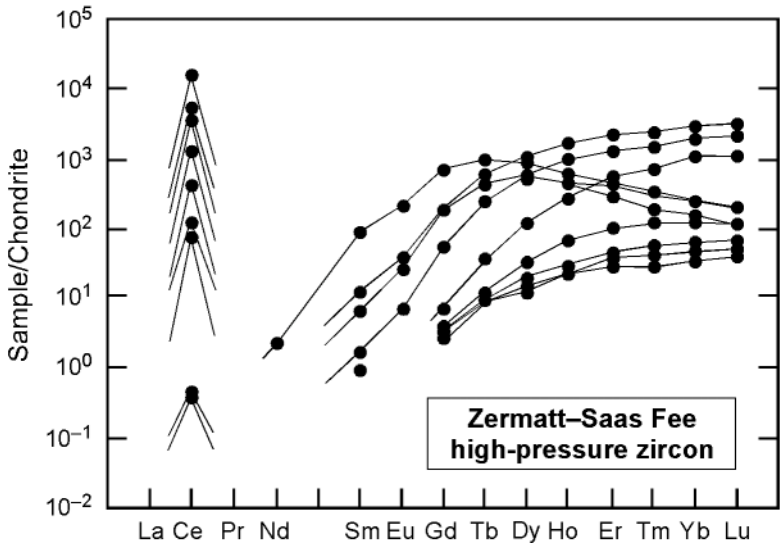

Figure 8. Chondrite-normalized REE patterns for metamorphic zircon from Lago di Cignana (Zermatt–Saas Fee, European Alps) eclogitic-grade metasediments. The zircons grew in equilibrium with garnet and have extremely large positive Ce anomalies and relatively depressed HREE patterns. Figure after Rubatto (2002).

2001, 2002; Liu et al. 2002), the work of Schaltegger et al. (1999) and Rubatto (2002) relating the REE composition of new net-transfer/metamorphic zircon to specific stages of metamorphic petrogenesis means that zircon U–Pb isotopic ages can be linked with specific *P-T* conditions thus allowing direct assessment of the rate of tectonic and metamorphic processes.

The composition of metamorphic zircon in equilibrium with an anatectic melt does not differ greatly from igneous zircon. The zircons are enriched in trace-elements with ionic radii close to that of Zr (i.e., Hf, Y, U, P) and have steep REE patterns increasing from La to Lu with positive Ce and negative Eu anomalies (Fig. 9a). Such patterns are clearly distinguishable from REE patterns produced by sub-solidus growth with garnet (Figs. 8 and 9b). The metamorphic-melt zircons described by Rubatto et al. (2001) and Rubatto (2002) have relatively depleted MREE abundances that are attributed to similarly depleted abundances in the precipitating melt and not to co-crystallization with a REE-rich phase such as monazite. The only apparent systematic distinction between igneous zircon and metamorphic-melt zircon is the Th/U ratio, which is very low for the latter (<0.07, Rubatto 2002).

Solid-state recrystallization and dissolution-reprecpitation of protolith zircon and compositional changes

Metamorphic zircon may be produced by intra-grain "reworking" of protolith igneous or detrital zircon or previously formed metamorphic zircon. The processes of reworking are solid-state recrystallization and local dissolution-reprecipitation. These processes appear not to be significant at low metamorphic grades were non-metamict protolith zircon tends to survive, although it can be mechanically fractured (Wayne and Sinha 1992). At higher grades these processes create a variety of internal textures. These secondary textures have been described by Vavra et al. (1996, 1999), Schaltegger et al. (1999), Hoskin and Black (2000), Möller et al. (2002) and Rubatto (2002) and include the following:

Blurred primary zoning. Primary igneous oscillatory zoning may be blurred (or "faded") as a first indication of metamorphic disturbance of the structure.

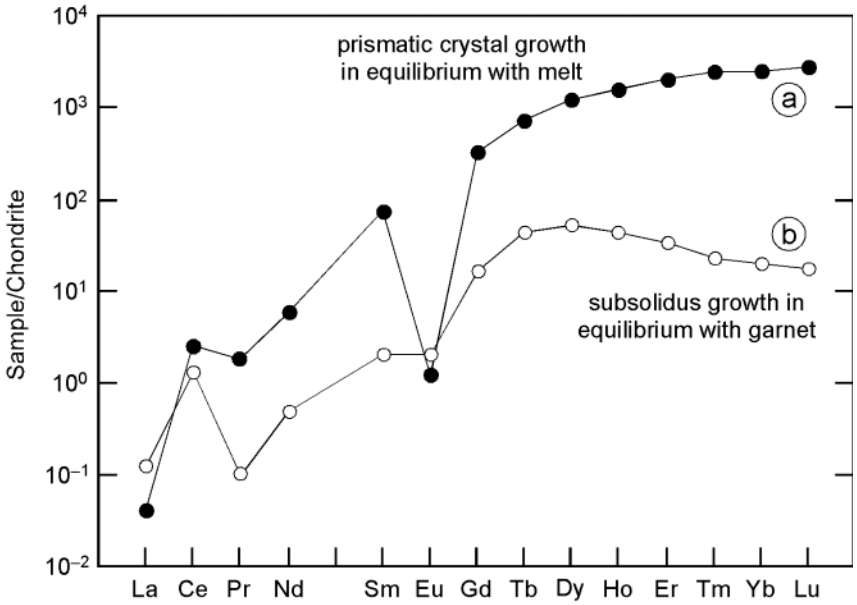

Figure 9. Chondrite-normalized representative REE patterns for metamorphic zircon equilibrated with a melt phase (a) and zircon equilibrated with garnet (b) under subsolidus conditions. Figure after Schaltegger et al. (1999).

Convoluted zoning. External parts of metamorphic zircon may show non-planar zoning formed by a series of low-CL and high-CL sinuous zones that may appear to be folded. This texture was called "flow zones" by Vavra et al. (1999) and Schaltegger et al. (1999). Individual zones can become discontinuous and truncated. The texture is considered to be the result of further convolution of blurred primary zoning (Hoskin and Black 2000).

Transgressive recrystallization. Local recrystallization of zircon under non-metamorphic conditions was described by Pidgeon (1992), Nemchin and Pidgeon (1997) and Pidgeon et al. (1998). The secondary texture produced is internally featureless, has sinuous and lobate edges, and cuts across other primary and secondary textures. Analogous textures in zircon from high-grade metamorphic rocks were described from Mount Sones, Antarctica (Black et al. 1986), Northwest Territories, Canada (van Breemen et al. 1987), Seve Nappes, Scandinavia (Williams and Claesson 1987), Vosges Mountains, France (Schaltegger et al. 1999) and the Georgetown Region, Australia (Hoskin and Black 2000). Although areas of transgressive recrystallization are generally internally featureless, they may preserve relics ("ghosts") of primary textures including oscillatory zoning. Transgressive recrystallized areas are separated from other structures by a grey-CL featureless recrystallization front (see Fig. 2 of Hoskin and Black 2000). In most examples, the recrystallization front appears to migrate from crystal pyramidal-terminations towards the interior of grains, although recrystallization may occur at locations away from crystal terminations, at domain boundaries or around inclusions (Figs. 7 and 10a).

The end result of transgressive recrystallization is complete recrystallization. Some zircon from high-grade rocks have no internal textures and are considered to have been fully recrystallized, for example the ~570 Ma gem-quality zircons in the Sri Lanka gem-gravels. Recrystallization has been proposed to occur in the solid-state without an essential role for a fluid-phase (Hoskin and Black 2000), although Tomaschek et al. (2003) provide strong evidence for an essential fluid-phase. Möller et al. (2002) argue for both fluid-present and fluid-absent zircon recrystallization in ultra-high-temperature granulites from southwest Norway. Evidence for solid-state, isochemical (on a

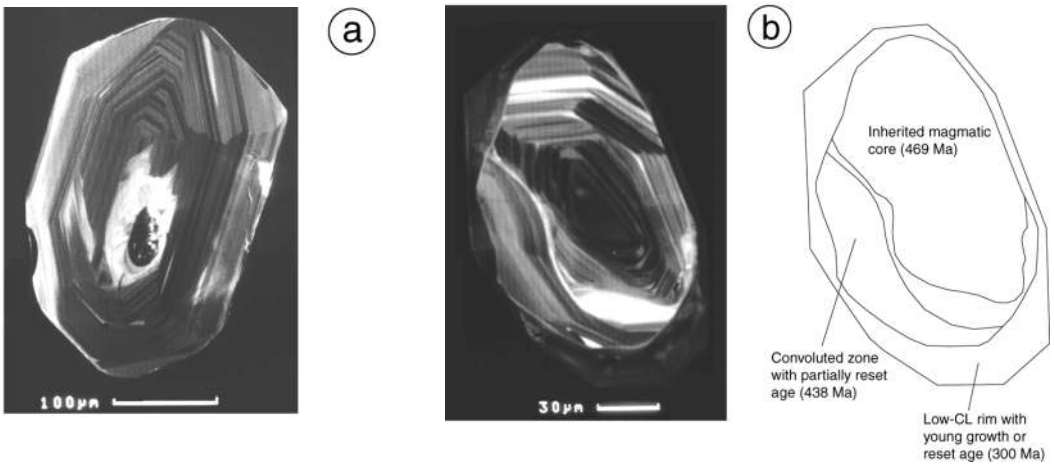

Figure 10. Zircon recrystallization textures: (a) *top row:* recrystallization around a mineral inclusion. The area of recrystallization is delineated by bright-CL as in Figure 7; (b) *bottom row:* various recrystallization features in a granulite-grade zircon with a large inherited core (469 Ma): convoluted zone with partially reset U–Pb age (438 Ma); low-CL rim with reset U–Pb age (300 Ma). Figure after Schaltegger et al. (1999).

crystal-scale) recrystallization, is the preservation of primary textures, in particular ghost textures, and the "mixed" isotopic ages (Figs. 10b and 11a) and trace-element compositions measured from these.

Recrystallization of protolith zircon has the effect of purging non-essential structural constituent cations (ESCs; Zr, Hf, Si) from the recrystallized structure. Cations with ionic radii significantly different from Zr (and Hf) and Si are purged from the structure. This was documented by Hoskin and Black (2000) for zircon from a meta-granitoid gneiss (Fig. 11). Eightfold coordinated Th^{4+} has a larger ionic radius than U^{4+} and appears to be preferentially purged with a consequent decrease in the Th/U ratio. This decrease correlates with a decrease in the $^{207}Pb/^{206}Pb$ age of the zircon; the youngest cluster of ages with Th/U <0.1 (solid circles, Fig. 11a) represent completely recrystallized zircon. Within a single crystal, trace elements are partitioned between recrystallized areas and the recrystallization front described above, enriching the front and depleting the recrystallized areas (see Er vs. P, U vs. Th and P vs. U plots, Fig. 11b). An exception to this trend is observed for Hf (see U vs. Hf plot, Fig. 11b). Hafnium enrichment is a feature of recrystallized zircons described by Pan (1997), where protolith zircon is recrystallized to trace-element-depleted–Hf-enriched zircon and xenotime according to the reaction $(Zr,Hf,Y,REE)(Si,P)O_4 \rightarrow (Zr,Hf)SiO_4 + (Y,REE)PO_4$. This reaction mechanism, with the addition of U-Th-silicates as a product, is advocated by Tomaschek et al. (2003) (Fig. 12). Normalized REE patterns for co-existing recrystallized zircon and recrystallization fronts in a single zircon (Fig. 11c) reveal the recrystallized zircon to be relatively depleted in the LREE and MREE with no measurable difference for Tm, Yb or Lu. As for Th and U, this is interpreted to be a consequence of cation size difference to Zr, which is greatest for the LREE and least for the HREE.

Differential trace-element purging as a function of cation ionic radii provides an explanation for U–Pb isotopic resetting and preservation of the Lu–Hf isotopic system. The ~570 Ma Sri Lanka zircons which on the basis of internal textures and likely source lithology are believed to be recrystallized, have a young U–Pb age (~570 Ma) and a Hf isotope model age of ~1.5 Ga (Kinny et al. 1991).

The mechanism or driving-force for recrystallization proposed by Hoskin and Black (2000) is thermoactivated grain-boundary and defect migration and the reduction of structural strain imposed by substituted trace elements. It is an observation that recrystallization is typically initiated at crystal terminations where trace elements are typically enriched above abundances at prism faces. Ghost

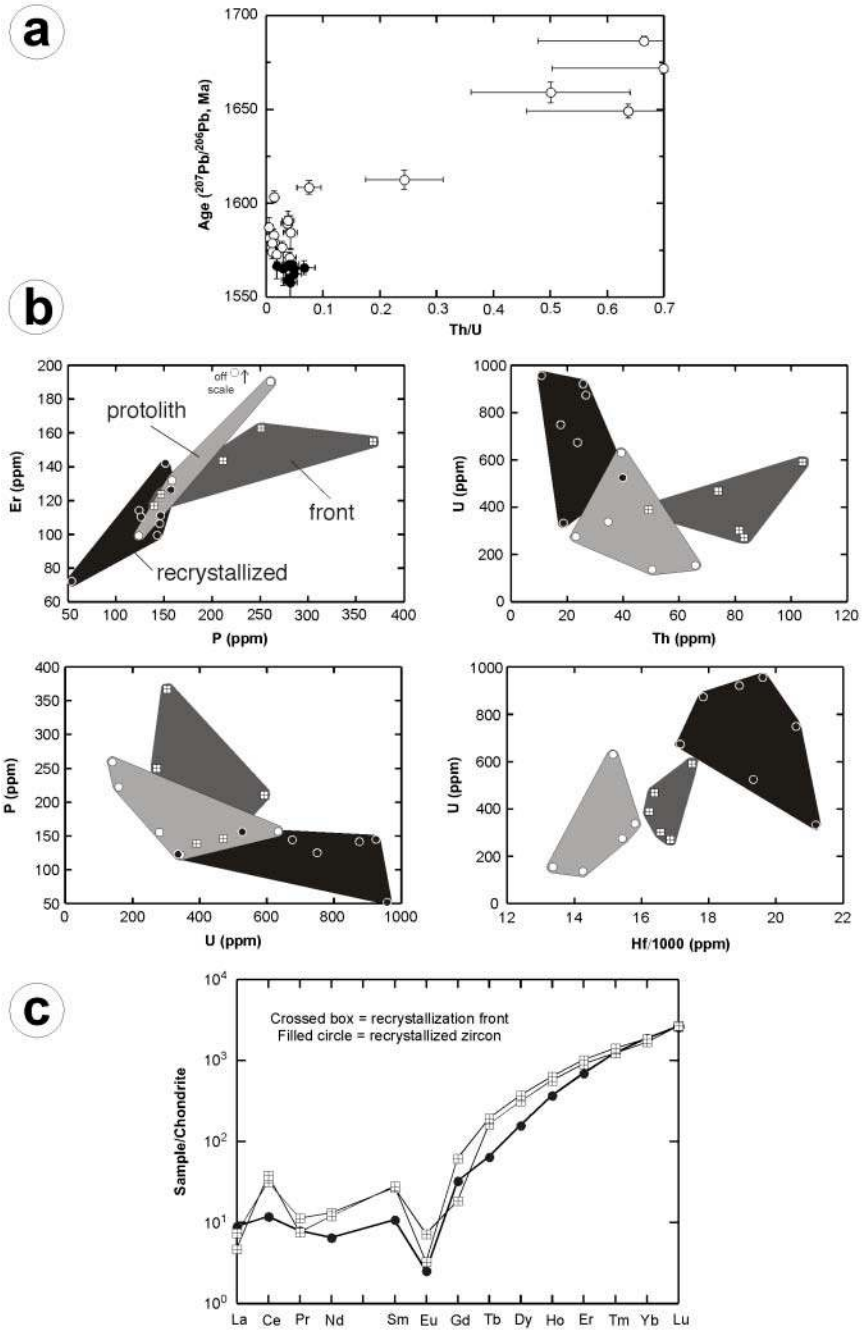

Figure 11. Isotope and trace-element characteristics of zircon from a meta-granitoid gneiss, northern Queensland, Australia. The zircon are partially to fully recrystallized. Internal textures observed in most crystals include primary igneous (protolith) zircon, recrystallized areas, and between these two, a recrystallization front: (a) ^{207}Pb/^{206}Pb age versus Th/U plot indicating the decrease in both age and Th/U ratio as recrystallization proceeds from partial (open symbols) to complete (solid symbols). Error bars are 1σ; (b) element–element plots for internal structures; (c) chondrite-normalized REE plots for recrystallized zircon and recrystallization front in a single crystal. Figure after Hoskin and Black (2000).

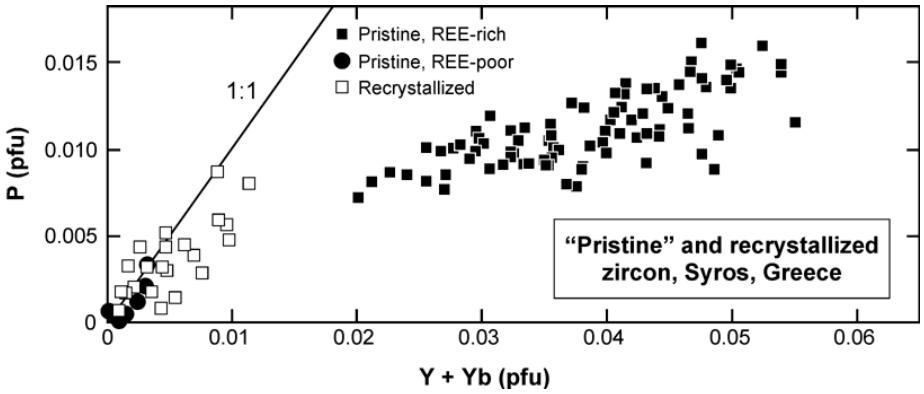

Figure 12. Phosphorus (per formula unit, pfu) versus Y + Yb (pfu) composition of zircon from a felsic meta-tuff, Syros, Greece. Pristine zircon with Y + Yb greater than 0.02 pfu (solid square symbols) have experienced partial to complete recrystallization with consequent reduction of P, Y and Yb (open square symbols). Pristine zircon that is relatively REE-poor has not recrystallized (solid circle symbols). The solid line joins points of equal P (pfu) and Y + Yb (pfu). Figure after Tomaschek et al. (2003).

textures—the preservation of primary textures, albeit altered—do not favor a mechanism of local dissolution-reprecipitation. This is, however, the mechanism proposed by Tomaschek et al. (2003) (see also Putnis 2002, p. 694), whose recrystallized zircon do not preserve ghost textures, but have ~10 vol % porosity and remnant fluid-inclusion voids, both of which are not observed in unaltered ("pristine") crystals. The fluid responsible for dissolution in this case, must also have been responsible for the dissolution of the numerous apatite and silicate inclusions in those crystals.

The role of metamictization in recrystallization by dissolution-reprecipitation and compositional change has been evaluated experimentally and analytically by Geisler et al. (2001, 2002, 2003). Metamict zircon is more susceptible to dissolution-reprecipitation because of the occurrence of amorphous zones and metamictization-induced fractures which allow fluid infiltration and exchange (Valley et al. 1994). Geisler et al. (2001), in hydrothermal experiments at 450°C, 1.3 kbar and 2 M $CaCl_2$ solution, recrystallized metamict rims on Sri Lanka zircon. The reaction rims are partially to fully structurally recovered (i.e., crystalline, not metamict) and have sharp, curved and transgressive boundaries with unreacted zircon (Putnis 2002, Fig. 5 therein) similar to the secondary transgressive textures produced geologically. Compositionally, the rims have lost radiogenic Pb, Zr, Si and have a reduced Th/U ratio, and have been enriched relative to unreacted zircon in Ca, Al (Geisler et al. 2002) and an undefined "water species". Metamict areas in zircon from the eastern Desert, Egypt, have exchanged with a low-temperature (120-200°C) aqueous fluid and are heavily enriched in Ca, Al, Fe, Mn, LREE and a water species, and have lost Zr, Si and radiogenic Pb (Geisler et al. 2003). Although these data indicate that fluid-induced recrystallization and isotopic resetting or discordance might be important in nature, the applicability of the results to higher-grade metamorphic zircon is unclear especially because many of the experimentally produced secondary textures are not commonly observed naturally, if at all. This may be because fluid-present recrystallization can also occur for non-metamict zircon, producing different secondary textures but similar compositional change including lowering of Th/U ratios and U–Pb isotope resetting (e.g., Liati and Gebauer 1999, Rubatto et al. 1999, Schaltegger et al. 1999).

HYDROTHERMAL ZIRCON

Zircon formation is not commonly associated with hydrothermal activity. In fact, it has been documented to be replaced by the hydrothermal deposition of zirconolite, $(Ca,REE)ZrTi_2O_7$, and a series of REE-phosphates, carbonates and oxides-hydroxides (Gieré 1996). Consequently, early

reports of hydrothermal zircon were met with skepticism (Claoué-Long et al. 1990, Corfu and Davis 1991, Claoué-Long et al. 1992). Since the early 1990s there have been an increasing number of reports of hydrothermal zircon. Williams et al. (1996) documented an extended episode of fluid-flow during high-grade metamorphism by dating hydrothermal zircon from metamorphic quartz veins. Most reports of hydrothermal zircon, however, are from relatively low- to medium-temperature and low-pressure events associated with economic deposition of Au and other metals and these occurrences are considered below.

Hydrothermal zircon has been reported from Archean massive sulfide deposits (Yeats et al. 1996), vein-type Archean gold deposits in Canada, China and Australia (Claoué-Long et al. 1990, Kerrich and King 1993, Li et al. 1997, Yeats et al. 1996), and a variety of shear and terrane suture zones (Wyoming Province, Mueller et al. 1996; Kaapvaal Craton, Flowers 2000; Newfoundland Appalachians, Ramezani et al. 2000). Despite these studies no consistent picture of hydrothermal zircon textures and composition has been forthcoming; anhedral and faceted morphologies and zoned and unzoned crystals have been described as hydrothermal, as have low common-Pb and high common-Pb zircon. The hydrothermal zircon of Yeats et al. (1996) fall into two distinct sub-populations on the basis of REE composition (P.W.O. Hoskin, unpublished data) even though there is no distinction between them on the basis of morphology or internal textures and they form a single U–Pb age population. The igneous-style normalized REE patterns and the absence of fluid-inclusions brings into question the interpretation of these zircons as being hydrothermal. In fact, the occurrence of zircon in hydrothermal veins, or even as inclusions in hydrothermal minerals, is not evidence enough that the zircon is likewise hydrothermal. For example, Hack et al. (1998) separated zircon from near-monomineralic hydrothermal quartz veins (with accessory Au-Bi alloys and zircon) and on the basis of U–Pb isotope ages concluded that the zircon was xenocrystic from the host meta-sediment. Zircon from the assimilated host-rock was the only mineral phase not to completely dissolve into the quartz-depositing hydrothermal fluid.

No such doubt of origin exists in the case of zircons described by Kerrich and King (1993) which contain inclusions of Au and fluid, or for fluid-inclusion-rich and "stringer" zircon from the Sierra Blanca Peaks, Texas (Rubin et al. 1989). Other criteria for identifying zircon as hydrothermal may include: "spongy texture" due to a high frequency of fluid-inclusions (Hoskin et al. 1998); high common-Pb abundance (Watson et al. 1997); and elevated abundances of F, LREE, Nb, Ta and other incompatible elements (Rubin et al. 1989, Hoskin et al. 1998) as expected from the type of fluids that mobilize Zr (Taylor et al. 1980, Rubin et al. 1993, Campbell 1998).

Trace-element characteristics of hydrothermal zircon have been described in two independent studies both of granitoids in eastern Australia (Boggy Plain Zoned Pluton, Hoskin et al. (1998) and Hoskin (1999); Mole Granite, Pettke et al. (2001) and Schaltegger et al. (2001)). Both granitoids are W-mineralized by fluids derived by magmatic differentiation (the Mole Granite is also Sn-mineralized). Despite similar geographical and geological contexts, the zircon compositional characteristics are contradictory (Fig. 13). Hydrothermal zircon from the Boggy Plain Zoned Pluton is enriched in the REE relative to igneous zircon which has a typical igneous-style normalized REE pattern. In particular, the LREE are enriched by about two orders of magnitude, although the Ce-anomaly is decreased from Ce/Ce* = 32-77 for igneous zircon to Ce/Ce* = 0.06-4.2 for hydrothermal zircon. Enrichment in the LREE is accompanied by enrichment in F, Y, Sc, Nb, Ta, Hf, Th and U (with fluid-inclusion hosted Mo, W and Au detected in some analyses). In contrast, REE abundances of hydrothermal zircon from the Mole Granite are depleted by 1 to 3 orders of magnitude relative to igneous zircon and have an increased Ce-anomaly. The significance of these contradictory data is presently unknown, but may reflect different hydrothermal mineral assemblages: in the Boggy Plain Zoned Pluton, hydrothermal zircon is precipitated with scheelite, ilmenite, rutile and yttrobetafite, whilst in the Mole Granite, hydrothermal zircon precipitated with monazite, thorite and xenotime. Differences in fluid origins, composition and fO_2 are also likely to be important.

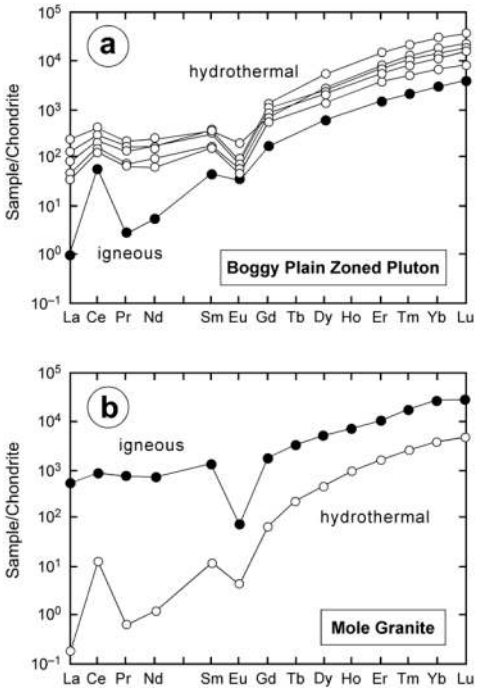

Figure 13. Chondrite-normalized REE patterns of hydrothermal zircon. The zircon crystallized under conditions of high aqueous-fluid activity at the end of magmatic crystallization. Both examples are from mineralized intrusions in southeast Australia: (a) Boggy Plain Zoned Pluton (Hoskin et al. 1998); (b) Mole Granite (Pettke et al., unpublished data).

CONCLUSIONS AND OUTLOOK

Zircon is a host of geochemically important elements that are used for isotopic age determination and for petrogenetic process investigation. Unaltered igneous zircon generally contains less that 1 wt % of the REE and Y. Chondrite normalized abundance patterns are HREE enriched relative to the LREE and rise steeply from La to Lu. If zircon saturates early in the differentiation of a magma and fractionates, it tends to deplete the residual melt in the HREE. The normalized REE pattern varies little and zircon from very different source-rocks have very similar REE patterns. There appears to be no systematic compositional differences between zircon from different parageneses. The implications of this are that back-calculation of melt compositions from zircon trace-element abundances and partition coefficients, as well as provenance investigations and source-rock "finger-printing," can lead to spurious results. Although zircon with a mantle-affinity has distinct REE characteristics, it is not clear why crustal zircons are so similar. This is an obvious area for future research that must include experimental and high-quality analytical studies of trace-element substitution mechanisms. It seems reasonable to predict that H^+ and OH, as well as interstitial Al, play a significant, yet currently under-recognized role in charge-balancing Y and REE in zircon. An important feature of the normalized igneous zircon REE pattern is the occurrence of Ce and Eu-anomalies, both of which are probably fully or partly controlled by oxygen fugacity. Experimental investigations of these anomalies should improve current understanding of why the anomalies exist and what they can tell us about magma genesis.

Metamorphic zircon appears to better retain a record of petrogenesis. A few studies have demonstrated that cogenetic zircon and garnet growth produces a normalized HREE pattern where the HREE in zircon dramatically drop away from expected values due to competition from co-crystallizing garnet. More dramatic patterns may be observed for zircon that has grown in the presence of metamorphic xenotime, monazite or an epidote-group mineral. Surprisingly, there is no clear understanding of why the Th/U ratio of metamorphic zircon is often ~0.01 or lower, when apparently igneous zircon has a value of >0.5. It may be that this is due to the presence of a fluid during metamorphic crystallization and in some cases due to differential expulsion of cations from zircon

during recrystallization. The phenomenon of sector zoning has received theoretical treatment from Watson and Liang (1995) and its occurrence is fairly well understood. The occurrence of sector zoning due to intersectoral trace-element partitioning may be temperature sensitive and could be calibrated as a thermometer.

ACKNOWLEDGMENTS

Discussions with John Hanchar, Ian Williams, Trevor Ireland, Hugh O'Neill, Richard Armstrong, Rodney Grapes, Richard Wysoczanski, Wayne Taylor, Thorsten Geisler, Chris Ballhaus, Michael Palin and Robert Linnen helped clarify various aspects of this contribution. We thank Paul Ribbe for his professional assistance.

REFERENCES

Ahrens LH (1965) Some observations on the uranium and thorium distributions in accessory zircon from granitic rocks. Geochim Cosmochim Acta 29:711-716

Ahrens LH, Cherry RD, Erlank AJ (1967) Observations on the Th-U relationship in zircons from granite rocks and from kimberlites. Geochim Cosmochim Acta 31:2379-2387

Ahrens LH, Erlank AJ (1969) Hafnium. *In* Handbook of Geochemistry. Vol 2, part 5, sections B-O. Wedepohl KH (ed) Springer-Verlag, Berlin–Heidelberg–New York

Amelin Y, Zaitsev AN (2002) Precise geochronology of phoscorites and carbonatites: the critical role of U-series disequilibrium in age interpretations. Geochim Cosmochim Acta 66:2399-2419

Bacon CR (1989) Crystallization of accessory phases in magmas by local saturation adjacent to phenocrysts. Geochim Cosmochim Acta 53:1055-1066

Baker DR, Conte AM, Freda C, Ottolini L (2002) The effect of halogens on Zr diffusion and zircon dissolution in hydrous metaluminous granitic melts. Contrib Mineral Petrol 142:666-678

Ballard JR, Palin JM, Campbell IH (2002) Relative oxidation states of magmas inferred from Ce(IV)/Ce(III) in zircon: application to porphyry copper deposits of northern Chile. Contrib Mineral Petrol 144:347-364

Barbey P, Allé P, Brouand M, Albarède F (1995) Rare-earth patterns in zircons from the Manaslu granite and Tibetan Slab migmatites (Himalaya): insights in the origin and evolution of a crustally-derived granite magma. Chem Geol 125:1-17

Baruah J, Kotoky P, Sarma JN (1995) Zircons in Jhanji river sediments. Bull Pure Appl Sci, Section F: Geol Sci 14F:35-40

Bea F (1996) Residence of REE, Y, Th and U in granites and crustal protoliths; implications for the chemistry of crustal melts. J Petrol 37:521-552

Bea F, Montero P (1999) Behaviour of accessory phases and redistribution of Zr, REE, Y, Th and U during metamorphism and partial melting of metapelites in the lower crust: an example from the Kinzigite Formation of Ivrea-Verbano, NW Italy. Geochim Cosmochim Acta 63:1133-1153

Bea F, Pereira MD, Stroh A (1994) Mineral/leucosome trace-element partitioning in a peraluminous migmatite (a laser ablation-ICP-MS study). Chem Geol 117:291-312

Belousova EA, Griffin WL, Pearson NJ (1998) Trace element composition and cathodoluminescence properties of southern African kimberlitic zircons. Mineral Mag 62:355-366

Belousova EA, Griffin WL, O'Reilly SY, Fisher NJ (2002) Igneous zircon: trace element composition as an indicator of source rock type. Contrib Mineral Petrol 143:602-622

Benisek A, Finger F (1993) Factors controlling the development of prism faces in granite zircons: A microprobe study. Contrib Mineral Petrol 114:441-451

Bingen B, Austrheim H, Whitehouse M (2001) Ilmenite as a source for zirconium during high-grade metamorphism? Textural evidence from the Caledonides of W. Norway and implications for zircon geochronology. J Petrol 42:355-375

Black LP, Williams IS, Compston W (1986) Four zircon ages from one rock: the history of a 3930 Ma-old granulite from Mount Sones, Enderby Land, Antarctica. Contrib Mineral Petrol 94:427-437

Blagojevic N, Garrett RF, Stampfl APJ, Cai Z, Lai B, Legnini DG, Rodrigues W (2000) Synchrotron X-ray microprobe analysis of radioactive trace elements in zircon and ilmenite. *In* Speciation, Techniques and Facilities for Radioactive Materials at Synchrotron Light Sources. NEA Workshop Proc, Grenoble, France, p 199-206

Bussy F, Cadoppi P (1996) U-Pb zircon dating of granitoids from the Dora-Maira massif (western Italian Alps). Schweiz Mineral Petrogr Mitt 76:217-233

Cameron KL, Hanson GN (1982) Rare earth element evidence concerning the origin of voluminous mid-Tertiary rhyolitic ignimbrites and related volcanic rocks, Sierra Madre Occidental, Chihuahua, Mexico. Geochim Cosmochim Acta 46:1489-1503

Campbell LS (1998) Zircon-fluid interaction in the Bayan Obo REE-Nb-Fe ore deposit, Inner Mongolia, China. *In*

Water-Rock Interaction, WRI-9. Arehart GB, Hulston JR (eds) AA Balkema, Rotterdam, p 521-523
Caruba R, Iacconi P (1983) Les zircons des pegmatites de Narssârssuk (Groëland)—l'eau et les groupments OH dans les zircons meamictes. Chem Geol 38:75-92
Chen YD, Williams IS (1990) Zircon inheritance in mafic inclusions from Bega Batholith granites, southeastern Australia: an ion microprobe study. J Geophys Res 95:17,787-17,796
Cherniak DJ, Hanchar JM, Watson EB (1997a) Rare-earth diffusion in zircon. Chem Geol 134:289-301
Cherniak DJ, Hanchar JM, Watson EB (1997b) Diffusion of tetravalent cations in zircon. Contrib Mineral Petrol 127:383-390
Chesner CA (1998) Petrogenesis of the Toba Tuffs, Sumatra, Indonesia. J Petrol 39:397-438
Chen YD, Williams IS (1990) Zircon inheritance in mafic inclusions from Bega Batholith granites, southeastern Australia: an ion microprobe study. J Geophys Res 95:17,787-17,796
Chiarenzelli JR, McLelland JM (1993) Granulite facies metamorphism, palaeo-isotherms and disturbance of the U-Pb systematics of zircon in anorogenic plutonic rocks from the Adirondack Highlands. J Metamor Geol 11:59-70
Claoué-Long JC, King RW, Kerrich R (1990) Archaean hydrothermal zircon in the Abitibi greenstone belt: constraints on the timing of gold mineralisation. Earth Planet Sci Lett 98:109-128
Claoué-Long JC, King RW, Kerrich R (1992) Reply to comment by F. Corfu and D.W. Davis on "Archaean hydrothermal zircon in the Abitibi greenstone belt: constraints on the timing of gold mineralisation". Earth Planet Sci Lett 109:601-609
Corfu F, Davis DW (1991) Comment on "Archean hydrothermal zircon in the Abitibi greenstone belt: constraints on the timing of gold mineralization" by J.C. Claoué-Long, R.W. King and R. Kerrich. Earth Planet Sci Lett 104:545-552
Correia Neves JM, Lopes Nunes JE, Sahama ThG (1974) High hafnium members of the zircon-hafnon series from the granite pegmatites of Zambézia, Mozambique. Contrib Mineral Petrol 48:73-80
Crocombette JP (1999) Theoretical study of point defects in crystalline zircon. Phys Chem Minerals 27:138-143
Currie KL, Knutson J, Temby PA (1992) The Mud Tank carbonatite complex, central Australia—an example of metasomatism at mid-crustal levels. Contrib Mineral Petrol 109:326-339
Dabard MP, Loi A, Peucat JJ (1996) Zircon typology combined with Sm-Nd whole-rock isotope analysis to study Brioverian sediments from the Armorican Massif. Sed Geol 101:243-260
de la Rosa JD, Jenner GA, Castro A (2002) A study of inherited zircons in granitoid rocks from the South Portuguese and Ossa-Morena Zones, Iberian Massif: support for the exotic origin of the South Portuguese Zone. Tectonophysics 352:245-256
Degeling H, Eggins S, Ellis DJ (2001) Zr budgets for metamorphic reactions, and the formation of zircon from garnet breakdown. Mineral Mag 65:749-758
Dickinson JE Jr, Hess PC (1982) Zircon saturation in lunar basalts and granites. Earth Planet Sci Lett 57:336-344
Dowty E (1980) Crystal growth and nucleation theory and the numerical simulation of igneous crystallization. *In* Physics of Magmatic Processes. Hargraves RB (ed) Princeton University Press, Princeton, New Jersey, p 419-485
Es'kova EM (1959) Geochemistry of Nb and Ta in the nepheline syenite massifs of the Vishnevyie Mountains. Geokhimiya 2:130-139 (in Russian)
Evans OC, Hanson GN (1993) Accessory-mineral fractionation of rare-earth element (REE) abundances in granitoid rocks. Chem Geol 110:69-93
Farges F (1996) Does Zr-F "complexation" occur in magmas? Chem Geol 127:253-268
Feng R, Machado N, Ludden J (1993) Lead geochronology of zircon by laser probe inductively coupled plasma mass spectrometry (LP-ICP-MS). Geochim Cosmochim Acta 57:3479-3486
Finch RJ, Hanchar JM, Hoskin PWO, Burns PC (2001) Rare-earth elements in synthetic zircon: Part 2. A single-crystal X-ray study of xenotime substitution. Am Mineral 86:681-689
Flowers RM (2000) Structural and geochronological investigation of the Archean basement along the projection of the Vredefort discontinuity, Vredefort impact structure, Kaapvaal Craton, South Africa. MS thesis, University of Utah, Provo, Utah
Fowler A, Prokoph A, Stern R, Dupuis C (2002) Organization of oscillatory zoning in zircon: Analysis, scaling, geochemistry, and model of a zircon from Kipawa, Quebec, Canada. Geochim Cosmochim Acta 66:311-328
Fraser G, Ellis D, Eggins S (1997) Zirconium abundance in granulite-facies minerals, with implications for zircon geochronology in high-grade rocks. Geology 25:607-610
Frondel C (1953) Hydroxyl substitution in thorite and zircon. Am Mineral 38:1007-1018
Fujimaki H (1986) Partition coefficients of Hf, Zr, and REE between zircon, apatite, and liquid. Contrib Mineral Petrol 94:42-45
Geisler T, Pidgeon RT, van Bronswijk W, Kurtz R (2002) Transport of uranium, thorium, and lead in metamict zircon under low-temperature hydrothermal conditions. Chem Geol 191:141-154
Geisler T, Rashwan AEA, Rahn MKW, Poller U, Zwingmann H, Pidgeon RT, Schleicher H, Tomaschek F (2003) Low-temperature hydrothermal alteration of natural metamict zircons from the Eastern Desert, Egypt. Mineral Mag (in press)

Geisler T, Schleicher H (2000) Improved U-Th-total Pb dating of zircons by electron microprobe using a simple new background modeling procedure and Ca as a chemical criterion of fluid-induced U-Th-Pb discordance in zircon. Chem Geol 163:269-285

Geisler T, Ulonska M, Schleicher H, Pidgeon RT, van Bronswijk W (2001) Leaching and differential recrystallization of metamict zircon under experimental hydrothermal conditions. Contrib Mineral Petrol 141:53-65

Gieré R (1996) Formation of rare earth minerals in hydrothermal systems. *In* Rare earth minerals: chemistry, origin and ore deposits. Jones AP, Wall F, Williams CT (eds) Chapman Hall, p 105-150

Gorz H (1974) Microprobe studies of inclusions and compilation of minor and trace elements in zircons from the literature. Chemie der Erde 33:326-357

Griffin WL, Wang X, Jackson SE, Pearson NJ, O'Reilly SY, Xu X, Zhou X (2002) Zircon chemistry and magma mixing, SE China: *in situ* analysis of Hf isotopes, Tonglu and Pingtan igneous complexes. Lithos 61:237-269

Gromet LP, Silver LT (1983) Rare earth element distributions among minerals in a granodiorite and their petrogenetic implications. Geochim Cosmochim Acta 47:925-939

Guo J, O'Reilly SY, Griffin WL (1996) Zircon inclusions in corundum megacrysts: I. Trace element geochemistry and clues to the origin of corundum megacrysts in alkali basalts. Geochim Cosmochim Acta 60:2347-2363

Hack AC, Mavrogenes JA, Hoskin PWO, Scott RJ (1998) A turbidite-hosted gold(-bismuth) quartz vein deposit, Union Hill Mine, Maldon, central Victoria. Geol Soc Austral (abstr) 49:194

Halden NM, Hawthorne FC (1993) The fractal geometry of oscillatory zoning in crystals: application to zircon. Am Mineral 78:1113-1116

Halden NM, Hawthorne FC, Campbell JL, Teesdale WJ, Maxwell JA, Higuchi D (1993) Chemical characterization of oscillatory zoning and overgrowths in zircon using 3 MeV μ-PIXE. Can Mineral 31:637-647

Hanchar JM, Finch RJ, Hoskin PWO, Watson EB, Cherniak DJ, Mariano AN (2001) Rare earth elements in synthetic zircon: Part I. Synthesis, and rare-earth element and phosphorous doping of zircon. Am Mineral 86:667-680

Hanchar JM, Hoskin PWO (1998) Mud Tank Carbonatite, Australia, zircon. Soc Lum Micros Spec News 10:2-3

Hanchar JM, Miller CF (1993) Zircon zonation patterns as revealed by cathodoluminescence and backscattered electron images: implications for interpretation of complex crustal histories. Chem Geol 110:1-13

Hanchar JM, Rudnick RL (1995) Revealing hidden structures: the application of cathodoluminescence and backscattered electron imaging to dating zircon from lower crustal xenoliths. Lithos 36:289-303

Harrison TM, Watson EB (1983) Kinetics of zircon dissolution and zirconium diffusion in granitic melts of variable water content. Contrib Mineral Petrol 84:66-72

Heaman LM, Bowins R, Crocket J (1990) The chemical composition of igneous zircon suites: implications for geochemical tracer studies. Geochim Cosmochim Acta 54:1597-1607

Hermann J, Rubatto D, Korsakov A, Shatsky VS (2001) Multiple zircon growth during fast exhumation of diamondiferous, deeply subducted continental crust (Kokchetav massif, Kazachstan). Contrib Mineral Petrol 141:66-82

Hidaka H, Shimizu H, Adachi M (2002) U-Pb geochronology and REE geochemistry of zircons from Palaeoproterozoic paragneiss clasts in the Mesozoic Kamiaso conglomerate, central Japan: evidence for an Archean provenance. Chem Geol 187:279-293

Hinton RW, Meyer C (1991) Ion probe analysis of zircon and yttrobetafite in a lunar granite. Lunar Planet Sci 22:575-576

Hinton RW, Upton BGJ (1991) The chemistry of zircon: variations within and between large crystals from syenite and alkali basalt xenoliths. Geochim Cosmochim Acta 55:3287-3302

Hirata T, Nesbitt RW (1995) U-Pb isotope geochronology of zircon: evaluation of the laser probe inductively coupled plasma mass spectrometry technique. Geochim Cosmochim Acta 59:2491-2500

Hoffmann C (1981) Chi-square testing of zircon populations from an Archean granite-greenstone terrain, Minas Gerais, Brazil. Neues Jahrb Mineral Abh 140:202-220

Holten T, Jamtveit B, Meakin P, Cortini M, Blundy J, Austrheim H (1997) Statistical characteristics and origin of oscillatory zoning in crystals. Am Mineral 82:596-606

Hoskin PWO (1998) Minor and trace element analysis of natural zircon ($ZrSiO_4$) by SIMS and laser ablation ICPMS: a consideration and comparison of two broadly competitive techniques. J Trace Microprobe Tech 16:301-326

Hoskin PWO (1999) SIMS determination of μg g^{-1}-level fluorine in geological samples and its concentration in NIST SRM 610. Geostand News: J Geostand Geoanal 23:69-76

Hoskin PWO (2000) Patterns of chaos: Fractal statistics and the oscillatory chemistry of zircon. Geochim Cosmochim Acta 64:1905-1923

Hoskin PWO, Black LP (2000) Metamorphic zircon formation by solid-state recrystallization of protolith igneous zircon. J Metamor Geol 18:423-439

Hoskin PWO, Ireland TR (2000) Rare earth element chemistry of zircon and its use as a provenance indicator. Geology 28:627-630

Hoskin PWO, Kinny PD, Wyborn D (1998) Chemistry of hydrothermal zircon: investigating timing and nature of water-rock interaction. *In* Water-Rock Interaction, WRI-9. Arehart GB, Hulston JR (eds) AA Balkema, Rotterdam, p 545-548

Hoskin PWO, Kinny PD, Wyborn D, Chappell BW (2000) Identifying accessory mineral saturation during differentiation in granitoid magmas: an integrated approach. J Petrol 41:1365-1396

Hoskin PWO, Rodgers KA (1996) Raman spectral shift in the isomorphous series $(Zr_{1-x}Hf_x)SiO_4$. Eur J Solid State Inorg Chem 33:1111-1121

Hower JC, Ruppert LF, Eble CF (1999) Lanthanide, yttrium, and zirconium anomalies in the Fire Clay coal bed, Eastern Kentucky. Intl J Coal Geol 39:141-153

Ireland TR, Wlotzka F (1992) The oldest zircons in the solar system. Earth Planet Sci Lett 109:1-10

Jackson SE, Longerich HP, Dunning GR, Freyer BJ (1992) The application of laser-ablation microprobe; inductively coupled plasma-mass spectrometry (LAM-ICP-MS) to in situ trace-element determinations in minerals. Can Mineral 30:1049-1064

Jain JC, Neal CR, Hanchar JM (2001) Problems associated with the determination of rare earth elements of a "gem" quality zircon by inductively coupled plasma-mass spectrometry. Geostand News: J Geostand Geoanal 25:229-237

Jeffries TE, Pearce NJG, Perkins WT, Raith A (1996) Chemical fractionation during infrared and ultraviolet laser ablation inductively coupled plasma mass spectrometry; implications for mineral microanalysis. Anal Comm 33:35-39

Katayama I, Masahito O, Yoshihide O (2002) Mineral inclusions in zircon from diamond-bearing marble in the Kokchetav Massif, northern Kazakhstan. Eur J Mineral 14:1103-1108

Katayama I, Maruyama S, Parkinson C, Terada K, Sano Y (2001) Ion micro-probe U-Pb zircon geochronology of peak and retrograde stages of ultrahigh-pressure metamorphic rocks from the Kokchetav massif, northern Kazachstan. Earth Planet Sci Lett 188:185-198

Kempe U, Gruner T, Nasdala L, Wolf D (2000) Relevance of cathodoluminescence for the interpretation of U-Pb zircon ages, with example of an application to a study of zircons from the Saxonian Granulite Complex, Norway. *In* Cathodoluminescence in Geosciences. Pagel M, Barbin V, Blanc P, Ohnenstetter D (eds) Springer, Berlin, p 415-455

Keppler H (1993) Influence of fluorine on the enrichment of high field strength trace elements in granitic rocks. Contrib Mineral Petrol 114:479-488

Kerrich R, King R (1993) Hydrothermal zircon and baddeleyite in Val d'Or Archean meothermal gold deposits: characteristics, compositions, and fluid-inclusion properties, with implications for timing of primary gold mineralization. Can J Earth Sci 30:2334-2352

Kinny PD, Compston W, Williams IS (1991) A reconnaissance ion-probe study of hafnium isotopes in zircons. Geochim Cosmochim Acta 55:849-859

Köhler H (1970) Die änderung der Zirkonmorphologie mit dem differentiationsgrad eines Granits. Neues Jahrb Mineral Mh 9:405-420

Konzett J, Armstrong RA, Sweeny RJ, Compston W (1998) The timing of MARID metasomatism in the Kaapvaal mantle: an ion probe study of zircons from MARID xenoliths. Earth Planet Sci Lett 160:133-145

Kopchenova YV, Mineyeva IG, Mineyev DA (1974) Calcium and sodium cyrtolite from albitite bodies in the Ukraine. Doklady Trans USSR Acad Sci Earth Sci 217:116-119

Köppel V, Grünenfelder M (1971) A study of inherited and newly formed zircons from paragneisses and granitised sediments of the Strona-Ceneri-zone (Southern Alps). Schweiz Mineral Petrogr Mitt 51:385-409

Köppel V, Sommerauer J (1974) Trace elements and the behaviour of the U—Pb system in inherited and newly formed zircons. Contrib Mineral Petrol 43:71-82

Kornacki AS, Fegley B Jr (1986) The abundance and relative volatility of refractory trace elements in Allende Ca, Al-rich inclusions: implications for chemical and physical processes in the sola nebula. Earth Planet Sci Lett 79:217-234

Koschek G (1993) Origin and significance of the SEM cathodoluminescence from zircon. J Micros 171:223-232

Kostov I (1973) Zircon morphology as a crystallogenetic indicator. Kristal Tech 8:11-19.

Kresten P, Fels P, Berggren G (1975) Kimberlitic zircons—a possible aid in prospecting for kimberlites. Mineral Dep 10:47-56

Larsen LH, Poldervaart A (1957) Measurement and distribution of zircons in some granitic rocks of magmatic origin. Mineral Mag 31:544-564

Li J, Shen B, Mao D, Li S, Zhou H, Cheng Y (1997) Mineralization ages of the Jiapigou gold deposits, Jilin. Acta Geologica Sinica 71:180-188

Liati A, Gebauer D (1999) Constraining the prograde and retrograde *P-T-t* path of Eocene HP rocks by SHRIMP dating of different zircon domains: inferred rates of heating, burial, cooling and exhumation for central Rhodope, northern Greece. Contrib Mineral Petrol 135:340-354

Linnen RL, Keppler H (2002) Melt composition control of Zr/Hf fractionation in magmatic processes. Geochim Cosmochim Acta 66:3293-3301

Liu F, Xu Z, Liou JG, Katayama I, Masago H, Maruyama S, Yang J (2002) Ultrahigh-pressure mineral inclusions in zircons from gneissic core samples of the Chinese Continental Scientific Drilling Site in eastern China. Eur J Mineral 14:499-512

Maas R, Kinny PD, Williams IS, Froude DO, Compston W (1992) The Earth's oldest known crust: a geochronological and geochemical study of 3900-4200 Ma old detrital zircons from Mt. Narryer and Jack Hills, Western

Australia. Geochim Cosmochim Acta 56:1281-1300
Mahood G, Hildreth W (1983) Large partition coefficients for trace elements in high-silica rhyolites. Geochim Cosmochim Acta 47:11-30
McDonough WF, Sun S-S (1995) The composition of the Earth. Chem Geol 120:223-253
Meyer C, Yang SV (1988) Tungsten-bearing yttrobetafite in lunar granophyre. Am Mineral 73:1420-1425
Möller A, O'Brien PJ, Kennedy A, Kröner A (2002) Polyphase zircon in ultrahigh-temperature granulites (Rogaland, SW Norway): constraints for Pb diffusion in zircon. J Metamor Geol 20:727-740
Mueller PA, Wooden JL, Mogk DW, Nutman AP, Williams IS (1996) Extended history of a 3.5 Ga trondhjemitic gneiss, Wyoming Province, USA: evidence from U-Pb systematics in zircon. Precambrian Res 78:41-52
Murali AV, Parthasarathy R, Mahadevan TM, Sankar Das M (1983) Trace element characteristics, REE patterns and partition coefficients of zircons from different geological environments—A case study on Indian zircons. Geochim Cosmochim Acta 47:2047-2052
Nagasawa H (1970) Rare earth concentrations in zircon and their host dacites and granites. Earth Planet Sci Lett 9:359-364
Nasdala L, Beran A, Libowitzky E, Wolf D (2001) The incorporation of hydroxyl groups and molecular water in natural zircon ($ZrSiO_4$). Am J Sci 301:831-857
Nemchin AA, Pidgeon RT (1997) Evolution of the Darling Range Batholith, Yilgarn Craton, Western Australia: a SHRIMP zircon study. J Petrol 38:625-649
Nesbitt RW, Hirata T, Butler IB, Milton JA (1997) UV laser ablation ICP-MS: some applications in the Earth Sciences. Geostand News: J Geostand Geoanal 20:231-243
O'Hara MJ, Fry N, Prichard HM (2001) Minor phases as carriers of trace elements in non-modal crystal-liquid separation processes II: illustrations and bearing on behaviour of REE, U, Th and the PGE in igneous processes. J Petrol 42:1887-1910
Ono A (1976) Chemistry and zoning of zircon from some Japanese granitic rocks. J Japan Assoc Mineral Petrol Econ Geol 71:6-17
Pan Y (1997) Zircon- and monazite-forming metamorphic reactions at Manitouwadge, Ontario. Can Mineral 35:105-118
Paterson BA, Stephens WE, Herd DA (1989) Zoning in granitoid accessory minerals as revealed by backscattered electron imagery. Mineral Mag 53:55-62
Paterson BA, Stephens WE, Rogers G, Williams IS, Hinton RW, Herd DA (1992) The nature of zircon inheritance in two granite plutons. Trans Roy Soc Edinburgh: Earth Sci 83:459-471
Peck WH, Valley JW, Wilde SA, Graham CM (2001) Oxygen isotope ratios and rare earth elements in 3.3 to 4.4 Ga zircons: ion microprobe evidence for high δ18O continental crust and oceans in the Early Archean. Geochim Cosmochim Acta 65:4215-4229
Perkins WT, Pearce NJG, Fuge R (1992) Analysis of zircon by laser ablation and solution inductively coupled plasma mass spectrometry. J Anal Atomic Spec 7:611-616
Pettke T, Audétat A, Schaltegger U, Heinrich CA (2001) Zircon trace element chemistry by LA-ICP-MS: a monitor for the magmatic-to-hydrothermal evolution of a crystallizing pluton? J Conf Abstr 6:680
Pidgeon RT (1992) Recrystallisation of oscillatory zoned zircon: some geochronological and petrological implications. Contrib Mineral Petrol 110:463-472
Pidgeon RT, Nemchin AA, Hitchen GJ (1998) Internal structures of zircons from Archaean granites from the Darling Range batholith: implications for zircon stability and the interpretation of zircon U-Pb ages. Contrib Mineral Petrol 132:288-299
Poldervaart A (1955) Zircons in rocks, 1. Sedimentary rocks. Am J Sci 253:433-461
Poldervaart A (1956) Zircons in rocks, 2. Igneous rocks. Am J Sci 254:521-554
Poller U, Huth J, Hoppe P, Williams IS (2001) REE, U, Th, and Hf distribution in zircon from western Carpathian Variscan granitoids: a combined cathodoluminescence and ion microprobe study. Am J Sci 301:858-876
Pupin JP (1980) Zircon and granite petrology. Contrib Mineral Petrol 73:207-220
Pupin JP, Turco G (1972a) Une typologie originale du zircon accessoire. Bull Soc Fr Minéral Cristallogr 95:348-359
Pupin JP, Turco G (1972b) Application des données morphologiques du zircon accessoire en pétrologie endogène. C R Acad Sci Paris 275D:799-802
Pupin JP, Turco G (1972c) Le zircon accessoire en géothermométrie. C R Acad Sci Paris 274D:2121-2124
Putnis A (2002) Mineral replacement reactions: from macroscopic observations to microscopic mechanisms. Mineral Mag 66:689-708
Ramakrishnan SS, Gokhale KVGK, Subbarao EC (1969) Solid solubility in the system zircon-hafnon. Mater Res Bull 4:323-328
Ramezani J, Dunning GR, Wilson MR (2000) Geologic setting, geochemistry of alteration, and U-Pb age of hydrothermal zircon from the Silurian Stog'er Tight gold prospect, Newfoundland Appalachians, Canada. Explor Mining Geol 9:171-188
Remond G, Cesbron F, Chapoulie R, Ohnenstetter D, Rosques-Carmes C, Schoverer M (1992) Cathodoluminescence applied to the microcharacterization of mineral materials: a present status in experimentation and interpretation.

Scanning Micros 6:23-68
Roberts MP, Finger F (1997) Do U-Pb zircon ages from granulites reflect peak metamorphic conditions? Geology 25:319-322
Robie RA, Hemingway BS, Fisher JR (1979) Thermodynamic properties of minerals and related substances at 298.15 K and 1 bar (10^5 Pascals) pressure and at higher temperatures (reprinted with corrections). U S Geol Surv Bull
Romans PA, Brown LL, White JC (1975) An electron microprobe study of yttrium, rare earth and phosphorous distribution in zoned and ordinary zircon. Am Mineral 60:475-480
Rubatto D (2002) Zircon trace element geochemistry: partitioning with garnet and the link between U-Pb ages and metamorphism. Chem Geol 184:123-138
Rubatto D, Gebauer D (2000) Use of cathodoluminescence for U-Pb zircon dating by ion microprobe: some examples from the Western Alps. *In* Cathodoluminescence in Geosciences. Pagel M, Barbin V, Blanc P, Ohnenstetter D (eds) Springer, Berlin, p 373-400
Rubatto D, Gebauer D, Compagnoni R (1999) Dating of eclogite-facies zircons: the age of Alpine metamorphism in the Sesia-Lanzo zone (Western Alps). Earth Planet Sci Lett 167:141-158
Rubatto D, Williams IS, Buick IS (2001) Zircon and monazite response to prograde metamorphism in the Reynolds Range, central Australia. Contrib Mineral Petrol 140:458-468
Rubin JN, Henry CD, Price JG (1989) Hydrothermal zircons and zircon overgrowths, Sierra Blanca Peaks, Texas. Am Mineral 74:865-869
Rubin JN, Henry CD, Price JG (1993) The mobility of zirconium and other "immobile" elements during hydrothermal alteration. Chem Geol 110:29-47
Rupasinghe MS, Dissanayake CB (1987) The geochemistry and mineralogy of zircons from Sri Lanka. Bull Geol Soc Finland 59:3-19
Sano Y, Terada K, Fukuoka T (2002) High mass resolution ion microprobe analysis of rare earth elements in silicate glass, apatite and zircon: lack of matrix dependency. Chem Geol 184:217-230
Sawka WN (1988) REE and trace element variation in accessory minerals and hornblende from the strongly zoned McMurry Meadows Pluton, California. Trans Roy Soc Edinburgh: Earth Sci 79:157-168
Saxena SK (1966) Evolution of zircons in sedimentary and metamorphic rocks. Sedimentology 6:1-33
Schaltegger U, Audétat A, Pettke T, Heinrich CA (2001) Dating of magmatic and hydrothermal stages in a Sn-W-granite. J Conf Abstr 6:681
Schaltegger U, Fanning CM, Günther D, Maurin JC, Schulmann K, Gebauer D (1999) Growth, annealing and recrystallization of zircon and preservation of monazite in high-grade metamorphism: conventional and in-situ U-Pb isotope, cathodoluminescence and microchemical evidence. Contrib Mineral Petrol 134:186-201
Schreiber HD, Lauer HV, Thanyasir T (1980) The redox state of cerium in basaltic magmas: an experimental study of iron-cerium interactions in silicate melts. Geochim Cosmochim Acta 44:1599-1612
Scoates JS, Chamberlain KR (1995) Baddeleyite (ZrO_2) and zircon ($ZrSiO_4$) from anorthositic rocks of the Laramie anorthosite complex, Wyoming: petrologic consequences and U-Pb ages. Am Mineral 80:1317-1327
Shannon RD (1976) Revised effective ionic radii and systematic studies of inter-atomic distances in halides and chalcogenides. Acta Crystallogr A32:751-767
Shore M, Fowler AD (1996) Oscillatory zoning in minerals: a common phenomenon. Can Mineral 34:1111-1126
Shnyukov SE, Andreev AV, Savenok SP (2002) Monitoring of region-scale geological/metallogenic events on a basis of single-grain trace element geochemistry of zircon, monazite and apatite large detrital populations: Ukrainian Shield and some other regions as an example. Intl Symp Metallogeny Precam Shields, Kiev, Ukraine (abstr)
Shnyukov SE, Andreev AV, Belousova EA, Savenok SP (2002) X-ray fluorescence milliprobe analysis in geochemistry of accessory minerals: research potential in comparison with high spatial resolution analytical methods. Mineral Zh (Ukraine) 24:80-95 (in Russian)
Silver LT, Deutsch S (1963) Uranium-lead isotopic variations in zircons: a case study. J Geol 71:721-758
Snyder GA, Taylor LA, Crozaz G (1993) Rare earth element selenochemistry of immiscible liquids and zircon at Apollo 14: an ion probe study of evolved rocks on the Moon. Geochim Cosmochim Acta 57:1143-1149
Speer JA (1982) Zircon. Rev Mineral 5(2^{nd} edn):67-112
Sutherland FL, Bosshart G, Fanning CM, Hoskin PWO, Coenraads RR (2002) Sapphire crystallization, age and origin, Ban Huai Sai, Laos: age based on zircon inclusions. J Asian Earth Sci 20:841-849
Sutherland FL, Hoskin PWO, Fanning CM, Coenraads RR (1998) Models of corundum origin from alkali basalt terrains: a reappraisal. Contrib Mineral Petrol 133:356-372
Taylor RP, Strong DF, Kean BF (1980) The Topsoils igneous complex: Silurian-Devonian peralkaline magmatism in western Newfoundland. Can J Earth Sci 17:425-439
Thomas JB, Bodnar RJ, Shimizu N, Sinha AK (2002) Determination of zircon/melt trace element partition coefficients from SIMS analysis of melt inclusions in zircon. Geochim Cosmochim Acta 66:2887-2901
Tomaschek F, Kennedy A, Villa I, Lagos M, Ballhaus C (2003) Zircons from Syros, Cyclades, Greece—recrystallisation and mobilization of zircon during high pressure metamorphism. J Petrol (in press)
Uher P, Breiter K, Kleèka M, Pivec E (1998) Zircon in highly evolved Hercynian Homolka Granite, Moldanubian

Zone, Czech Republic: indicator of magma source and petrogenesis. Geologica Carpathica 49:151-160
Uher P, Cerny P (1998) Zircon in Hercynian granitic pegmatites of the western Carpathians, Slovakia. Geologica Carpathica 49:261-270
Upton BGJ, Hinton RW, Aspen P, Finch A, Valley JW (1999) Megacrysts and associated xenoliths: evidence for migration of geochemically enriched melts in the upper mantle beneath Scotland. J Petrol 40:935-956
Valley JW, Chiarenzelli JR, McLelland JM (1994) Oxygen isotope geochemistry of zircon. Earth Planet Sci Lett 126:187-206
Valley JW, Peck WH, King EM, Wilde SA (2002) A cool early Earth. Geology 30:351-354
van Breemen O, Henderson JB, Loveridge WD, Thompson PH (1987) U-Pb zircon and monazite geochronology and zircon morphology of granulites and granite from the Thelon Tectonic Zone, Healey Lake and Artillery Lake map areas, NWT. Current Research Part A, Geol Survey Canada Paper 87-1A:783-801
Vavra G (1990) On the kinematics of zircon growth and its petrogenetic significance: a cathodoluminescence study. Contrib Mineral Petrol 106:90-99
Vavra G (1993) A guide to quantitative morphology of accessory zircon. Chem Geol 110:15-28
Vavra G (1994) Systematics of internal zircon morphology in major Variscan granitoid types. Contrib Mineral Petrol 117:331-334
Vavra G, Gebauer D, Schmid R, Compston W (1996) Multiple zircon growth and recrystallisation during polyphase Late Carboniferous to Triassic metamorphism in granulites of the Ivrea Zone (Southern Alps): an ion microprobe (SHRIMP) study. Contrib Mineral Petrol 122:337-358
Vavra G, Schmid R, Gebauer D (1999) Internal morphology, habit and U-Th-Pb microanalysis of amphibolite-to-granulite facies zircons: geochronology of the Ivrea zone (Southern Alps). Contrib Mineral Petrol 134:380-404
Wark DA, Miller CF (1993) Accessory mineral behavior during differentiation of a granite suite: monazite, xenotime and zircon in the Sweetwater Wash pluton, southeastern California, U.S.A. Chem Geol 110:49-67
Wang X, Griffin WL, O'Reilly SY, Zhou XM, Xu XS, Jackson SE, Pearson NJ (2002) Morphology and geochemistry of zircons from late Mesozoic igneous complexes in coastal SE China: implicaitions for petrogenesis. Mineral Mag 66:235-251
Watson EB (1979) Zircon saturation in felsic liquids: experimental results and applications to trace element geochemistry. Contrib Mineral Petrol 70:407-419
Watson EB (1980) Some experimentally determined zircon/liquid partition coefficients for the rare earth elements. Geochim Cosmochim Acta 44:895-897
Watson EB (1996a) Dissolution, growth and survival of zircons during crustal fusion: Kinetic principles, geological models and implications for isotopic inheritance. Trans Roy Soc Edinburgh: Earth Sci 87:43-56. Also: Geol Soc Am Spec Paper 315:43-56
Watson EB (1996b) Surface enrichment and trace-element uptake during crystal growth. Geochim Cosmochim Acta 60:5013-5020
Watson EB, Cherniak DJ, Hanchar JM, HarrisonTM, Wark DA (1997) The incorporation of Pb into zircon. Chem Geol 141:19-31
Watson EB, Harrison TM (1983) Zircon saturation revisited: temperature and composition effects in a variety of crustal magma types. Earth Planet Sci Lett 64:295-304
Watson EB, Liang Y (1995) A simple model for sector zoning in slowly grown crystals: implications for growth rate and lattice diffusion, with emphasis on accessory minerals in crustal rocks. Am Mineral 80:1179-1187
Watson EB, Vicenzi EP, Rapp RP (1989) Inclusion/host relations involving accessory minerals in high-grade metamorphic and anatectic rocks. Contrib Mineral Petrol 101:220-231
Watt GR, Harley SL (1993) Accessory phase controls on the geochemistry of crustal melts and restites produced during water-undersaturated partial melting. Contrib Mineral Petrol 114:550-556
Wayne DM, Sinha AK (1988) Physical and chemical response of zircons to deformation. Contrib Mineral Petrol 98:109-121
Wayne DM, Sinha AK (1992) Stability of zircon U-Pb systematics in a greenschist-grade mylonite: an example from the Rockfish Valley Fault Zone, Central Virginia, USA. J Geol 100:593-603
Whitehouse MJ, Platt JP (2003) Dating high-grade metamorphism—constraints from rare-earth elements in zircon and garnet. Contrib Mineral Petrol (in press)
Wiedenbeck M, Allé P, Corfu F, Griffin WL, Meier M, Oberli F, von Quadt A, Roddick JC, Spiegel W (1995) Three natural zircon standards for U-Th-Pb, Lu-Hf, trace element and REE analyses. Geostand Newslett 19:1-23
Wilde SA, Valley JW, Peck WH, Graham CM (2001) Evidence from detrital zircons for the existence of continental crust and oceans on the Earth 4.4 Gyr ago. Nature 409:175-178
Williams IS, Buick IS, Cartwright I (1996) An extended episode of early Mesoproterozoic fluid flow in the Reynolds Range, central Australia. J Metamor Geol 14:29-47
Williams IS, Claesson S (1987) Isotopic evidence for the Precambrian provenance and Caledonian metamorphism of high grade paragneisses from the Seve Nappes, Scandinavian Caledonides II. Ion microprobe zircon U-Th-Pb. Contrib Mineral Petrol 97:205-217

Williford RE, Weber WJ, Devanathan R, Cormak AN (1999) Native vacancy migrations in zircon. J Nuc Mater 273:164-170

Wopenka B, Jolliff BL, Zinner E, Kremser DT (1996) Trace element zoning and incipient metamictization in a lunar zircon: application of three microprobe techniques. Am Mineral 81:902-912

Wyborn D (1983) Fractionation processes in the Boggy Plain zoned pluton. PhD dissertation, Australian National University, Canberra

Yeats CJ, McNaughton NJ, Groves DI (1996) SHRIMP U-Pb geochronological constraints on Archean volcanic-hosted massive sulfide and lode gold mineralisation at Mount Gibson, Yilgarn Craton, Western Australia. Econ Geol 91:1354-1371

Yusoff M (2002) EDXRF as an important tool in the selective leaching of uranium and thorium from contaminated zircon. 51st Ann Denver X-ray Conf, Colorado (abstr)

Zeck HP, Williams IS (2002) Inherited and magmatic zircon from Neogene Hoyazo cordierite dacite, SE Spain—anatectic source rock provenance and magmatic evolution. J Petrol 43:1089-1104

Zinner E, Crozaz G (1986) A method for the quantitative measurement of rare earth elements in the ion microprobe. Intl J Mass Spect Ion Proc 69:17-38